

**FABRICATION AND CHARACTERIZATION OF COBALT PIGMENTED  
ANODIZED ZINC FOR PHOTOCATALYTIC APPLICATION**

**JUDITH CHEBWOGEN**

**A RESEARCH THESIS SUBMITTED TO THE INSTITUTE OF POST  
GRADUATE STUDIES OF KABARAK UNIVERSITY IN PARTIAL  
FULFILLMENT OF THE REQUIREMENT FOR THE AWARD OF MASTER OF  
SCIENCE IN PHYSICS**

**KABARAK UNIVERSITY**

**NOVEMBER, 2019**

## **DECLARATION**

This research thesis is my original work prepared with no other than the indicated sources and to the best of my knowledge has not been presented elsewhere for any award in any institution.

Signed: \_\_\_\_\_

Date: \_\_\_\_\_

Judith Chebwogen

GMP/M/2394/11/16

## RECOMMENDATION

To the institute of Postgraduate Studies:

The research thesis titled “**Fabrication and characterization of Cobalt pigmented anodized Zinc for photocatalytic application**” and written by **Judith Chebwogen** is presented to the Institute of Postgraduate Studies of Kabarak University. We have reviewed the research thesis and recommend it be accepted in partial fulfillment of the requirement for award of the degree of Master of Science in Physics.

Signed: \_\_\_\_\_

Date: \_\_\_\_\_

Dr. Christopher Mkiema Maghanga  
Department of Physical and Biological Sciences  
Kabarak University, Kenya

Signed: \_\_\_\_\_

Date: \_\_\_\_\_

Prof. Maurice Mghendi Mwamburi  
Department of Physics  
University of Eldoret, Kenya

**COPYRIGHT**

@ 2019

Chebwojen Judith

All rights reserved. No part of this Thesis may be reproduced or transmitted in any form by means of either mechanical, including recording, photocopying or any other information retrieval or storage system without permission in writing from the author or Kabarak University.

## **ACKNOWLEDGEMENT**

I thank God for His guidance, protection, strength, good health and the power of mind all through this study. My sincere gratitude to the International Science Programme (ISP) of Uppsala, Sweden for facilitating my research work, travel and stay in Lusaka-Zambia. It would not have been easy for me to do this work without your extraordinary support. The success of this study was achieved with the input of my supervisors; Dr. Christopher Maghanga and Prof Mghendi Mwamburi. I appreciate their expert advice and encouragement throughout this study. I also thank Dr Onesmus Munyati, Dr Hatwaambo and Prof Reccab Manyala from the University of Zambia. I am thankful to them for the skillful guidance, inspiration and support throughout my stay in Zambia. I am grateful to Kabarak University from which I did my coursework. I also thank the University of Zambia who hosted me and allowed me to do my research from their institution. I will not forget to mention the school of natural sciences from which I worked. The technician in the solid state laboratory Mr. Edmond Bundala, the technicians in the Chemistry department, UNZA workshop and my fellow students Juliah Rotich, Lameck Tembo, Happy Mabo, Oday Chibala, Cynthia Bwalya and Isabel Chisulo for their support. I am appreciative to my parents, my husband, children, sisters and brothers for all the unceasing support and encouragement they gave me during the course of my study. Finally, thanks to everyone who directly or indirectly made this study a success.

## **DEDICATION**

This work is dedicated to my much-loved parents Mr. and Mrs. Richard Koske, my husband Leonard Cheruiyot and children Angel and Angie. I also dedicate this to my brothers and sister, George, Winny, Enock and Edwin and their families.

## ABSTRACT

Population growth and urbanization have led to water scarcity and pollution which is a health hazard not only to human but also the ecosystem in general. This has necessitated coming up with ways of treating water before consumption. Photocatalysis has proved to be one of the most promising cheap techniques, which involve chemical utilization of solar energy.  $\text{TiO}_2$  widely used in photocatalysis absorbs a narrow range of the solar spectrum compared to  $\text{ZnO}$ . In this regard, this study aimed at preparing and optimizing Cobalt pigmented  $\text{ZnO}$  which is applicable in photocatalytic water treatment. The objectives in this study were to fabricate zinc oxide ( $\text{ZnO}$ ) thin films by anodization, pigment the fabricated films with varying Cobalt concentrations, characterize the fabricated films optically and to investigate the Cobalt pigmented  $\text{ZnO}$  performance in the methylene blue degradation under UV light irradiation. Mirror polished Zinc plates were sonicated in ethanol and rinsed. Anodization was done at room temperature in 0.5M oxalic acid at a constant voltage of 10V for 60 minutes and Cobalt electrodeposited in the films. Post deposition treatment was done at 250°C. Optical properties of the films were studied using a UV-VIS- NIR spectrophotometer in the solar range of 300nm-2500nm. The photocatalytic activity of the fabricated films was studied in Methylene Blue solution degradation in the presence of UV light irradiation for 5 hours. Cobalt pigmentation was observed to reduce reflectance and optical band gap from 3.34eV to 3.10eV indicating good photocatalytic properties. In this study,  $\text{ZnO}$  film pigmented with Cobalt for 20s was found to be the most photocatalytic with a rate constant of  $0.0317\text{hr}^{-1}$  hence had the optimum Cobalt concentration for photocatalytic water treatment. This can be applied in small scale water purification.

**Key words:** *photocatalysis, anodization, zinc oxide, pigmentation, post deposition treatment, optical properties*

## Table of Contents

<b>DECLARATION</b> .....	ii
<b>RECOMMENDATION</b> .....	iii
<b>COPYRIGHT</b> .....	iv
<b>ACKNOWLEDGEMENT</b> .....	v
<b>DEDICATION</b> .....	vi
<b>ABSTRACT</b> .....	vii
<b>LIST OF FIGURES</b> .....	x
<b>LIST OF SYMBOLS, ACRONYMS AND ABBREVIATIONS</b> .....	xi
<b>OPERATIONAL DEFINITION OF TERMS</b> .....	xiii
<b>CHAPTER ONE</b> .....	1
<b>INTRODUCTION</b> .....	1
1.1 Introduction .....	1
1.2 Background to the study .....	1
1.3 Statement of the problem .....	6
1.4 Purpose of the study .....	7
1.5 Objectives of the study .....	7
1.6 Research questions .....	7
1.7 Justification for the study .....	8
1.8 Scope of the study .....	9
1.9 Limitations of the study .....	9
1.10 Assumption of the study .....	9
<b>CHAPTER TWO</b> .....	10
<b>LITERATURE REVIEW</b> .....	10
2.1 Introduction .....	10
2.2 Empirical review of work done on pure and Cobalt doped <i>ZnO</i> .....	10
2.3 Theoretical review of ZnO and thin film optics .....	14
<b>CHAPTER THREE</b> .....	47
<b>RESEARCH DESIGN AND METHODOLOGY</b> .....	47
3.1 Introduction .....	47
3.2 Research design .....	47



3.3 Sample preparation.....	47
3.4 Instruments used in characterization of the films.....	49
3.5 Data collection procedure.....	52
3.6 Data analysis .....	52
<b>CHAPTER FOUR .....</b>	<b>57</b>
<b>DATA ANALYSIS, PRESENTATION AND DISCUSSION .....</b>	<b>57</b>
4.1 Introduction.....	57
4.2 Results and discussion of the study.....	57
<b>CHAPTER FIVE .....</b>	<b>77</b>
<b>SUMMARY, CONCLUSIONS AND RECOMMENDATIONS .....</b>	<b>77</b>
5.1 Introduction.....	77
5.2 Summary .....	77
5.3 Conclusions.....	77
5.4 Recommendations for further research .....	80
<b>REFERENCES .....</b>	<b>82</b>
<b>APPENDICES.....</b>	<b>89</b>
Appendix 1: Cobalt Deposit and Methylene Blue Standard Solution Data.....	89
Appendix 2: Kabarak University Introductory Letter.....	90
Appendix 3: Nacosti Introductory Letter.....	91
Appendix 4: Nacosti Permit Research .....	92
Appendix 5: Research Affiliation Approval.....	93

## LIST OF FIGURES

<b>Figure 1:</b> Photocatalyst e- and h+ generation and their possible reactions in aqueous solutions, Irani et al. (2016) .....	3
<b>Figure 2:</b> <i>ZnO</i> structures with grey spheres representing Oxygen atoms and black represent Zinc atoms, Espitia et al. (2012) .....	15
<b>Figure 3:</b> Schematic diagram for the experimental setup for anodization, Nemes et al. (2011)..	20
<b>Figure 4:</b> A diagram illustrating the interaction of light with a film supported by a substrate, KHELLADI and SARI (2013) .....	26
<b>Figure 5:</b> Air mass 1.5 direct normal irradiance and hemispherical tilted reflectance 37° sun facing surface, ASTM G173-03 (2012) .....	30
<b>Figure 6:</b> Schematic diagram showing direct band gap transition, Rathod (2014) .....	35
<b>Figure 7:</b> Schematic diagram showing indirect band gap transitions, Rathod (2014).....	36
<b>Figure 8:</b> Diagram showing <i>ZnO</i> photocatalytic mechanism, Ong et al. (2018).....	42
<b>Figure 9:</b> Heterogeneous surface catalysis steps, Ertl (1990).....	44
<b>Figure 10:</b> Schematic diagram of the double beam spectrophotometer, Taylor (2010).....	51
<b>Figure 11:</b> An illustration of fitting of the experimental to simulated spectra using the SCOUT software .....	58
<b>Figure 12:</b> Graph showing the variation of calculated amounts of Cobalt deposited (g) and the deposition time (s).....	59
<b>Figure 13:</b> Measured reflectance as a function of wavelength for polished Zinc metal and as-deposited <i>ZnO</i> film.....	61
<b>Figure 14:</b> Measured reflectance for Zinc and the <i>ZnO</i> films with different Cobalt concentrations.....	63
<b>Figure 15:</b> Change in integrated reflectance with increase in Cobalt concentration .....	64
<b>Figure 16:</b> Effect of Cobalt pigmentation on the <i>ZnO</i> absorption edge for some sampled films ...	65
<b>Figure 17:</b> Absorption coefficient ( $m^{-1}$ ) versus wavelength (nm) .....	66
<b>Figure 18 (a):</b> Refractive index, $n$ of the prepared films as a function of wavelength .....	68
<b>Figure 18 (b):</b> Extinction coefficient, $k$ of the prepared films as a function of wavelength.....	69
<b>Figure 19:</b> Graph showing the band gap analysis of the fabricated films .....	70
<b>Figure 20:</b> Methylene blue calibration curve.....	73
<b>Figure 21:</b> A graph of $\ln(C/C_0)$ versus time in minutes for sampled films .....	74
<b>Figure 22:</b> Effect of pigment concentration on rate constant ( $k$ ).....	75

## LIST OF SYMBOLS, ACRONYMS AND ABBREVIATIONS

$\alpha(\lambda)$	absorption coefficient as a function of wavelength
$\varepsilon(\infty)$	dielectric constant at high frequency
$\varepsilon(\omega)$	dielectric constant as a function of angular frequency
$\lambda$	wavelength
$\mu\text{m}$	micrometer
$\chi$	susceptibility
$\omega$	angular frequency of the radiation
$A(\lambda)$	absorbance as a function of wavelength
<b>AM0</b>	airmass 0
<b>AM1.5</b>	airmass 1.5
$c$	speed of light
<b>Co:ZnO</b>	Cobalt doped Zinc oxide
<b>DC</b>	Direct current
<b>EDX</b>	Energy Dispersive X-ray
$E_g$	energy band gap
<b>eV</b>	electron volt
<b>FTIR</b>	Fourier Transform Infrared Spectroscopy
$h$	planck's constant
$HO^*$	hydroxyl radical
$i$	imaginary number
$I_0$	total intensity of incident radiation
$I_A$	amount of light absorbed
$I_R$	amount of light reflected
$I_T$	amount of light transmitted
<b>k</b>	rate constant
$k(\omega)$	extinction coefficient as a function of angular frequency
<b>LEDs</b>	Light Emitting Diodes
<b>meV</b>	millielectron volt
<b>mg/l</b>	milligram per litre
$n$	refractive index
$n(\omega)$	refractive index as a function of angular frequency
$N(\omega)$	complex refractive index as a function of angular
frequency	
<b>NaOH</b>	Sodium Hydroxide
<b>Nb<sub>2</sub>O<sub>5</sub></b>	Niobium pentoxide
<b>nm</b>	nanometre
$O_2^*$	superoxide
<b>OJL</b>	O'Leary, S.K., Johnson, SR., Lim, P.K.
<b>PAH</b>	Polycyclic Aromatic Hydrocarbons
<b>pH</b>	potential of hydrogen

<b><math>R(\lambda)</math></b>	reflectance as function of wavelength
<b>RF</b>	Radio Frequency
<b>SEM</b>	Scanning Electron Microscopy
<b>SnO<sub>2</sub></b>	tin oxide
<b><math>T(\lambda)</math></b>	transmittance as a function of wavelength
<b>TCP</b>	trichlorophenol
<b>TEM</b>	Transmission Electron Microscopy
<b>TiO<sub>2</sub></b>	titanium dioxide
<b>UNDP</b>	United Nations Development Programme
<b>UNICEF</b>	United Nations International Children's Emergency Fund
<b>UNWWAP</b>	United Nations World Water Assessment Programme
<b>UV/VIS NIR</b>	ultraviolet-visible near infrared
<b>UV</b>	ultraviolet
<b>V<sub>2</sub>O<sub>5</sub></b>	Vanadium (V) oxide
<b>WHO</b>	World Health Organization
<b>WO<sub>3</sub></b>	Tungsten trioxide
<b>XPS</b>	X-ray Photoelectron Spectroscopy
<b>XRD</b>	X- Ray Diffractometer
<b><math>Zn(OH)_2</math></b>	Zinc hydroxide
<b>Zn</b>	Zinc
<b><math>Zn^{2+}</math></b>	Zinc ion
<b>ZnO</b>	zinc oxide
<b>ZnO:Co 10s</b>	Zinc oxide with Cobalt deposited for 10 seconds
<b>ZnO:Co 20s</b>	Zinc oxide with Cobalt deposited for 20 seconds
<b>ZnO:Co 30s</b>	Zinc oxide with Cobalt deposited for 30 seconds
<b>ZnO:Co 40s</b>	Zinc oxide with Cobalt deposited for 40 seconds
<b>ZnO:Co 50s</b>	Zinc oxide with Cobalt deposited for 50 seconds
<b>ZnO:Co 60s</b>	Zinc oxide with Cobalt deposited for 60 seconds
<b>ZrO<sub>2</sub></b>	zirconia
<b>ZT</b>	Zinc titanate

## OPERATIONAL DEFINITION OF TERMS

- Photocatalysis:** A photoreaction that takes place on the surface of a semiconductor catalyst.
- Anodization:** A process which forms of an oxide layer on certain metal surfaces and involves passing current through a chemical cell.
- Zinc oxide:** This is a semiconductor with a chemical formula ZnO whose band gap is wide almost 3.37eV.
- Pigmenting:** The introduction of an impurity into an intrinsic (pure) semiconductor to modify its properties.
- Post deposition treatment:** Subjecting a material to high temperatures where recrystallization occurs. The temperatures should be below its melting point.
- Optical properties:** The interaction of a material with light which includes its absorbance, transmittance and reflectance.

## **CHAPTER ONE**

### **INTRODUCTION**

#### **1.1 Introduction**

This chapter is short discussion on water pollution causes and the different ways of treating waste water. Photocatalysis which is the method used in the study has been described briefly in the background of the study. The problem that necessitated this study has been stated hence its purpose. The main and specific objectives have been stated consequently the research questions which guided the research. The justification and scope of the study are also presented. Lastly, the chapter gives the limitations and the assumptions made.

#### **1.2 Background to the study**

Population growth and urbanization have widely led to water contamination as stated by Qin et al. (2014). Contamination has resulted from waste water such as domestic and sewage water, water from fertilizer industries, food processing industries, slaughter houses, refineries and agriculture run-off which contain organic pollutants. According to Ghorani-Azam et al. (2016), these pollutants are a health hazard to human and also affect the ecosystem. Some pollutants like oil contain polycyclic aromatic hydrocarbons (PAH) some of which are carcinogenic while others like microbial pollutants from sewages cause infectious diseases to humans and also marine life.

Over 80% of polluted waste water is released to the environment with 95% released in some least developed countries as reported by United Nations World Water Assessment Programme, (UNWWAP) (2016). Inadequate sanitation is one of the causes of water pollution

and according to United Nations International Children's Emergency Fund (UNICEF) and World Health Organization (WHO); approximately 2.5 billion people in the world live with improper sanitation worldwide, UNICEF WHO (2014). Africa is among the continents in the world lagging behind in achieving sanitation and only 31% of the inhabitants had access to improved sanitation in the year 2006, UNICEF WHO (2008).

The contaminated waste water can be treated before discharge to the environment. Some of the water treatment methods used is reverse osmosis, sedimentation, filtration, distillation, coagulation and flocculation, chlorination, photocatalysis and aeration. Photocatalysis has proved to be one of the most promising ways of purifying waste water by chemically utilizing solar energy and results in degradation of hazardous organic pollutants, Hoffman et al. (1995).

Photocatalysis is a reaction that occurs at the surface of semiconductor catalysts called photocatalysts in presence of light with sufficient energy. This reaction results in toxic organic compounds in water being decomposed by pairs of electrons and holes that form in the semiconductor. These electrons and holes produced in the semiconductor react with oxygen and hydrogen in water through photo reduction and photo oxidation processes forming hydroxyl and superoxide radicals as illustrated in figure 1. The superoxide and hydroxyl radicals formed are very reactive species which degrade the organic compounds in water.

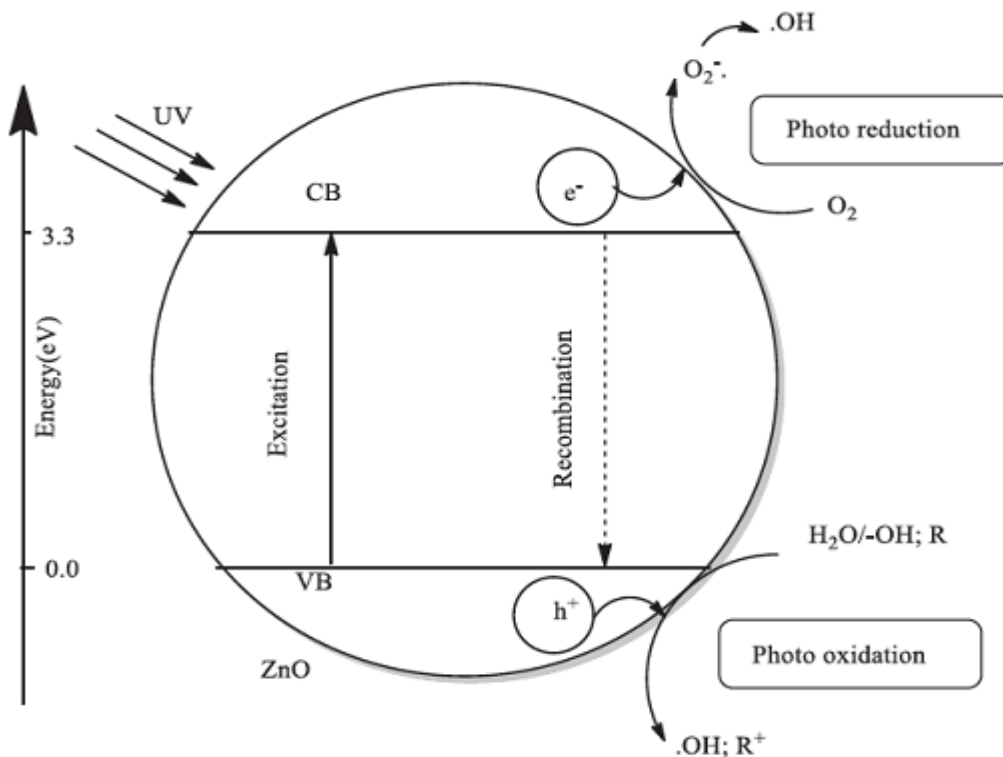


**Figure 1: Photocatalyst e<sup>-</sup> and h<sup>+</sup> generation and their possible reactions in aqueous solutions, Irani et al. (2016)**

Photocatalysis is one of the water treatment techniques that is preferred because of its efficiency, simplicity, possibility to use solar light thus reusable and its capability to mineralize pollutants into carbon (IV) oxide and water which are environment friendly, Prihod'ko and Soboleva (2013). Other than water treatment by degrading water pollutants, the other most common applications of photocatalysis are air purification, designing self-cleaning surfaces, in antibacterial action, hydrogen evolution through water splitting, sterilization and photo electrochemical conversion. All these applications involve the use of a semiconductors and semiconductor oxides which act as catalysts.

Zinc oxide (*ZnO*), tin oxide (*SnO<sub>2</sub>*), titanium dioxide (*TiO<sub>2</sub>*) and zirconia (*ZrO<sub>2</sub>*) have been attractive photocatalysts because of their effectiveness in photocatalytic degradation of



organic compounds in the presence of UV light, Chandrappa et al. (2012). Vinu and Madras (2012) and Kudo and Miseki (2009) have also reported that other semiconductor photocatalysts that can be used in degradation are niobium pentoxide ( $\text{Nb}_2\text{O}_5$ ), iron (iii) oxide ( $\text{Fe}_2\text{O}_3$ ), tungsten trioxide ( $\text{WO}_3$ ) and vanadium (v) oxide ( $\text{V}_2\text{O}_5$ ).

$\text{TiO}_2$  is among the semiconductor oxides that have been most studied and widely used for photocatalysis because it is effective, non-toxic, and structurally stable as stated by Fujishima et al. (2000) and Klosek and Raftery (2001). Its drawbacks however are that  $\text{TiO}_2$  absorbs only a relatively narrow range of the solar spectrum unlike  $\text{ZnO}$  which is capable of absorbing a broader range despite their similar band gap energies as indicated by Lizama et al. (2002).  $\text{TiO}_2$  also is only active by the UV region of the solar spectrum because of its wide band gap hence the need to modify it enabling it to absorb both in the Visible and UV regions. In this regard,  $\text{ZnO}$  which absorbs a broader range can be used as an alternative.  $\text{ZnO}$  is also non-toxic, cheap and readily available.

$\text{ZnO}$  is an n-type wide band gap semiconductor of about 3.37 eV at room temperature and a high exciton energy of 60 meV. Its multiple applications include electronics, pharmaceuticals, ceramics, surface coatings, agriculture and catalysis, Young (2016). Its wide band gap property makes it active only in the UV region of the solar spectrum, Iqbal et al. (2016) and its efficiency in photocatalysis is limited. However its band gap can be modified so as to enhance its efficiency by coupling with another semiconductor, doping or pigmenting with a metal, non-metal or a transition metal in order to increase its efficiency and quantum yield, Lavand and Malghe (2015) and amongst these doping is the most preferred.

Doping involves the addition of an impurity into a semiconductor to alter its properties. It can be achieved in different ways like diffusion, ion implantation or electrodeposition of the pigment ions or alloys. Diffusion is affected by temperature, concentration gradient and the substrate crystallographic orientation but electrodeposition is preferred because the dopant ions are deposited in the substrate lattice by an electric field. The applied voltage determines the depth in which the ions are deposited and their impact on the substrate which results in the substrate atoms knocked off from their lattice sites. Knocking off the substrate atoms leads to crystal lattice damage which can be cured by subjecting the doped substrate in high temperatures as the dopant ions are also made to move into the lattice sites and bond with the substrate atoms.

The impurity can be a metal, non-metal, transition metal or an alloy but doping *ZnO* with a transition metal is the most effective in reducing its band gap expanding the response to light from the UV to the visible range, Bahsi and Oral (2007). The dopant ions substitute Zn ions in the *ZnO* crystal lattice and become sites for recombination which trap the photogenerated electrons and holes preventing them from recombining hence enable the holes and electrons to help in the photocatalytic process. Among the transition metal dopants used, Cobalt is the most preferred because of its ionic radius (0.745 Å) which is almost similar to that of Zinc (0.74 Å), Woo et al. (2014).

Techniques such as hydrothermal, spray pyrolysis, sol gel, coprecipitation, Radio Frequency (RF) magnetron sputtering, Direct current (DC) and electrochemical anodization have been used to fabricate *ZnO* to different nanostructures. According to Chuah et al. (2012)

electrochemical anodization is preferred because it is an easy, low cost route in the synthesis of thin films. Anodization involves the formation of an oxide layer on certain metal surfaces through electrolysis which according to Voon et al. (2014), regulates the properties of the natural oxide layer and increases its thickness. Preparation of *ZnO* thin films by anodization has been reported by Yamaguchi et al. (1998), Basu et al. (2008), Ng et al. (2011), Voon et al. (2015) who fabricated thin films of *ZnO* through this method. In this study, we fabricated *ZnO* by electrochemical anodization, pigmented it with Cobalt by electrodeposition and optimized it for photocatalytic water treatment application.

### **1.3 Statement of the problem**

While water is vital for survival of living things, its pollution has become one of the major threats to life. Rapid population growth and urbanization has widely led to environmental challenges among them water scarcity and pollution. These threaten the fundamental human rights, such as the right to life, safe work, wellbeing, good health, as well as children protection and protection of the most vulnerable. The organic pollutants in water are hazardous and can cause diseases or death. Because of its global and national threat there is need for cheaper water treatment techniques such as photocatalysis.

Although  $\text{TiO}_2$  has been widely used in photocatalysis, its major drawback is its absorption of a narrow range of the solar spectrum compared to *ZnO* which can be used as an alternative. *ZnO* however is soluble in acid and hence may not be used in the treatment of acidic water. It is also active only in the UV region of the solar spectrum because of its wide band gap. This imposes the need to enhance its absorption capacity. Whereas doping has been stated as the

best method to improve absorption capacity, the dopant concentration beyond some point instead lowers absorption which in turn lowers photocatalysis. In this study, anodized Cobalt-pigmented *ZnO* thin film with optimum Cobalt concentration suitable for photocatalytic water treatment was investigated.

#### **1.4 Purpose of the study**

To prepare and optimize Cobalt pigmented *ZnO* which is applicable in photocatalytic water treatment.

#### **1.5 Objectives of the study**

The objectives in this study were to:

- i) Fabricate *ZnO* thin films by electrochemical anodization.
- ii) Pigment the fabricated *ZnO* thin films with varying concentrations of Cobalt.
- iii) Characterize optically the fabricated films so as to investigate the effect of Cobalt concentrations on the *ZnO* optical properties.
- iv) Evaluate the photocatalytic performance of the fabricated films in the methylene blue degradation under UV light irradiation hence identify the optimum Cobalt concentration to be used in Cobalt-pigmented *ZnO* photocatalysis.

#### **1.6 Research questions**

- i) How are *ZnO* thin films fabricated by electrochemical anodization?
- ii) How is Cobalt concentration deposited in the *ZnO* films varied?
- iii) What is the effect of changing Cobalt concentration in the *ZnO* optical properties?

- iv) What is the optimum Cobalt concentration in anodized *ZnO* suitable for photocatalytic water treatment?

### **1.7 Justification for the study**

There has been global environmental crisis in terms of water scarcity and pollution due to rapid population growth and urbanization. Several deaths have been reported resulting from water borne diseases such as cholera. These diseases most often affect the most vulnerable in the society whose access to clean water is inadequate. This necessitates seeking for cheaper and user friendly techniques which do not require well developed infrastructure to treat water. Photocatalysis which has demonstrated to be one of the promising techniques widely uses  $\text{TiO}_2$  as the photocatalyst but *ZnO* can be used as an alternative since it has a higher absorption capacity than  $\text{TiO}_2$ . The efficiency of *ZnO* in photocatalysis can be increased by pigmenting it with Cobalt although its photoactivity is determined by the amount of Cobalt in *ZnO*. Higher pigment concentrations limit photocatalysis indicating that there is an optimum concentration beyond which photocatalysis is lowered hence the need for investigation as reported in this study.

This study may provide a cheaper and user friendly way of treating water before consumption since the Cobalt pigmented *ZnO* films with the highest photocatalytic activity will be recommended for use in water treatment. Information from this study may add to already existing knowledge on Cobalt pigmented *ZnO* semiconductor in terms of its optical properties and its photocatalytic application.

### **1.8 Scope of the study**

The focus in this study is on optical properties of anodized Cobalt-pigmented *ZnO* and its photocatalytic activity. Therefore the findings in this study may not be generalized to other Cobalt doped *ZnO* films prepared using other deposition techniques.

### **1.9 Limitations of the study**

One of the limitations of the study is that there is little research that has been done on anodized Cobalt-pigmented *ZnO* hence the difficulty to compare findings with other similar works. However, comparison was done with Cobalt-doped *ZnO* deposited using other methods which may have different characteristics.

### **1.10 Assumption of the study**

This study made an assumption that the properties of the anodized Cobalt-pigmented *ZnO* were not affected by changes in the physical conditions such as changes in temperature, atmospheric pressure and humidity.

## CHAPTER TWO

### LITERATURE REVIEW

#### 2.1 Introduction

This chapter is a presentation of both empirical and theoretical review on pure and Cobalt doped *ZnO*. The first part of this chapter discusses the studies that have been done on pure and Cobalt doped *ZnO* and the second part is generally theory on *ZnO*, the interaction of light with thin films and photocatalysis.

#### 2.2 Empirical review of work done on pure and Cobalt doped *ZnO*

The study of *ZnO* nanoparticles photocatalytic activity which were fabricated by combustion method done by Nagaraju et al. (2017) who stated that *ZnO* has a band gap equivalent to 3.29 eV and SEM images showed almost spherical and agglomerated *ZnO* structures. The results in the methyl blue degradation under both sunlight and UV radiation showed *ZnO* as a good photocatalytic material. In Cobalt doped *ZnO*, Kuriakose (2014) studied improved photocatalytic activity of *ZnO* nanodisks and nanorods doped with Cobalt prepared by wet chemical method photocatalytic activity and reported that doping *ZnO* nanodisks and nanorods with Co improved their photocatalytic activity. They attributed the enhanced photocatalysis to enhanced nanodisks surface area and improvement of separation of charge because of optimal Cobalt doping which prevented the photogenerated holes and electrons from recombining hence enhanced photocatalysis.

Poongodi et al. (2015) studied the antibacterial and photocatalytic activities in visible light of nanostructured sol-gel synthesized *ZnO* thin films doped with Cobalt. They reported narrowing of the band gap and energy reduction from 3.32 to 3.05 eV for Cobalt

concentrations increased from 0wt% to 15wt%. The XRD results in this study revealed that the prepared films had a hexagonal wurtzite structure and further studies on the *ZnO* structure using XPS indicated that Cobalt was incorporated into the *ZnO* structure. Cobalt doping led to smaller *ZnO* grain sizes narrowing the band gap. In photocatalysis, *ZnO* doped with Cobalt was seen to be more photocatalytic in comparison to undoped *ZnO*.

While investigating the influence of Cobalt doping on optical properties and the structure of *ZnO* nanoparticles prepared using sol-gel method, Vanaja and Rao (2016) performed XRD, SEM and FTIR studies. The FTIR results showed the existence of Co-ZnO bonds which was an indication of Cobalt incorporation in the structure of *ZnO*. The XRD results also displayed a hexagonal wurtzite structure but in contrast to previous study by Poongodi et al. (2015) they observed an increase in the crystal size upon doping *ZnO* with Cobalt. This same increase in crystal size with Cobalt concentration from 0%wt to 5wt% had also been stated in an earlier study done by Oves et al. (2015) on the antimicrobial activity of *ZnO* nanoparticles doped with Cobalt.

In the synthesis by precipitation of highly efficient thin films of *ZnO* doped with Cobalt activated by visible light, Yildirim et al. (2016) varied the Cobalt concentrations from 0%wt to 5%wt. They investigated both structural, optical and photocatalytic properties of the films. They reported that both doped and pure ZnO films had a hexagonal wurtzite structure. In optical characterization, the films were highly transparent which decreased on doping. The films also exhibited a high visible region transmittance and a sharp decrease was observed at the UV region which corresponded to the absorption band edge. This edge was observed to



shift to longer wavelengths (Red shift) upon doping *ZnO* with Cobalt which was evident in the decrease of the band gap energy from 3.34eV to 3.10eV for pure *ZnO* and 5%wt Co concentration respectively. Cobalt doping was observed to have a positive effect in photocatalysis although only 3%wt Cobalt content was reported as the optimum in the Co:ZnO photocatalytic activity.

While investigating the effect on optical properties of Sol gel spin coated *ZnO* thin films doped with Cobalt, Borhani and Amrollahi (2017) increased the Cobalt doping concentration from 0%wt to 8%wt and observed that reflectance reduced when the Cobalt doping concentration was increased. A shift in the *ZnO* band edge towards the longer wavelengths (Red shift) was observed on doping. The absorption coefficient was observed to reduce with increasing wavelength and an increase with the extinction coefficient with Cobalt doping. The refractive index, *n* was observed to decrease from 2.46 to 2.15 for the pure *ZnO* and the 8%wt Cobalt doped *ZnO* respectively which they attributed to smaller crystallites formed. They also reported a reduction in the band gap from 3.17 to 3.05 eV for 0%wt and 8%wt Cobalt doped *ZnO*.

Kalpana et al. (2017) synthesized *ZnO* nanoparticles doped with Cobalt for photocatalytic activity through Co-precipitation method. The effect of Cobalt concentrations in the *ZnO* photocatalysis was investigated using 0.05%wt, 0.075%wt and 0.1%wt Cobalt concentrations. In the structural characterization, XRD results revealed that Cobalt ions substituted the  $Zn^{2+}$  ions in the *ZnO* lattice because there was no change in the structure on doping. The crystal size however was reported to increase as the Cobalt concentration was also increased. Unlike

the previous study by Yildirim et al. (2016) and Borhani and Amrollahi (2017), the absorption edge in the study was observed to shift towards lower wavelengths (Blue shift) as the Cobalt concentration was increased. Kaushik et al. (2013) in the study of the effect of Cobalt doping on *ZnO* nanocrystals magnetic, optical and structural properties had also reported an appreciable blue shift with Cobalt doping which resulted in band gap increase.

A study was conducted by Li et al. (2017) on  $Mn^{2+}$  and  $Co^{2+}$  doped *ZnO* nanowires visible light photocatalytic activity which they synthesized through hydrothermal method. The XRD diffraction peaks in this study indicated a hexagonal wurtzite structure in both Co-doped *ZnO* and Mn- doped *ZnO*. Similar to the other studies, a decrease in the band gap energy was reported from 3.25eV for pure *ZnO* to 3.20 eV and 3.11 eV for Mn-doped and Co-doped *ZnO* in that order. Photocatalytic studies on the films indicated an increase in photocatalysis in the doped films than pure films. Co-doped *ZnO* was however seen to be more efficient in Visible light photocatalytic activity than Mn-doped *ZnO*.

One of the latest studies on photocatalytic activity of Cobalt-doped thin films of *ZnO* done by Sutanto et al. (2017) fabricated the films by spray coating technique. They studied how Cobalt concentration affects photocatalytic activity, optical and structural properties of *ZnO* with the concentration of Cobalt increased from 0mol% to 10mol%. Similar to other studies, they reported that the films had a hexagonal wurtzite structure and there was successful incorporation of Cobalt ions into the lattice of *ZnO*. It was however reported in this study that the absorption band edge shifted towards lower wavelengths in contrast to what was observed by Kalpana et al. (2017). There was also a reduction in the band gap values from 3.02 to 3.00

eV for pure *ZnO* and 10mol% Co doped *ZnO* respectively resulting from the Red shift. The degradation of methylene blue under solar radiation was determined for all films and *ZnO* film with 4mol% of Co was observed to be the most photocatalytic.

Several studies have been conducted on Cobalt doped *ZnO* synthesized using different methods but anodized Cobalt doped *ZnO* for photocatalysis has not been reported. It is evident from the studies above that the effect of doping concentration on Cobalt doped *ZnO* optical and structural properties depends on the method of fabrication which has not been reported for anodized Cobalt doped *ZnO*. In photocatalysis, Yildirim et al. (2016) used precipitation method and obtained 3%wt Co as the optimal Cobalt concentration while Sutanto et al. (2017) used spray coating technique and found 4mol% Co indicating that this also depends on the method of preparation of the films. The optimal Cobalt concentration on anodized Cobalt doped *ZnO* has not been reported and hence the need to investigate in this study.

## **2.3 Theoretical review of ZnO and thin film optics**

### **2.3.1 Structure of *ZnO***

Zinc oxide with the chemical formula *ZnO* is an n-type semiconductor with a wide and direct band gap. It exists as large bulk single crystals and its crystals exist in three forms: the hexagonal wurtzite structure, rocksalt and cubic zincblende but the hexagonal wurtzite structure is the most common since it is more stable. Figure 2 shows the *ZnO* structures.

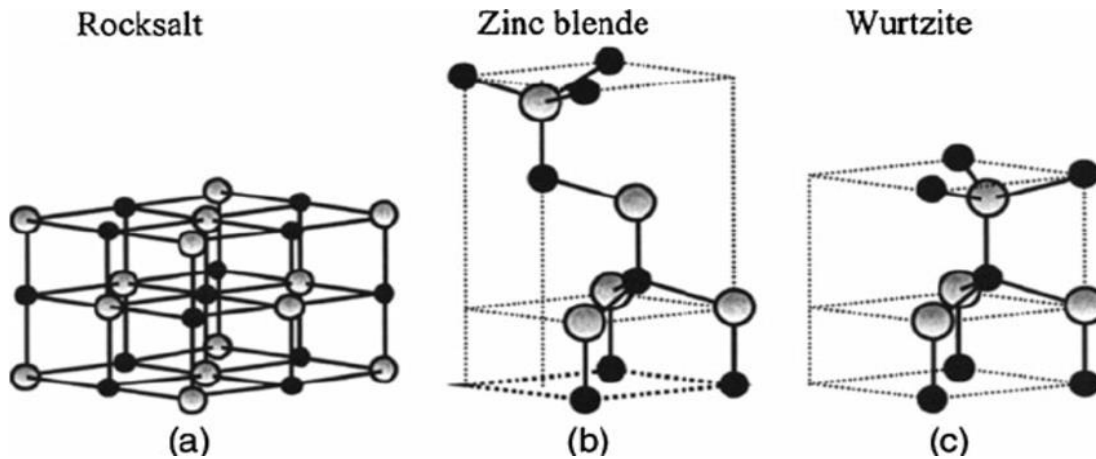


**Figure 2: *ZnO* structures with grey spheres representing Oxygen atoms and black represent Zinc atoms, Espitia et al. (2012).**

Due to its stability, hexagonal wurtzite structure has been widely reported. El et al. (2015) characterized Sol-gel synthesized *ZnO* nanoparticles doped with Cobalt. The results they obtained revealed that nanoparticles formed have a wurtzite single crystalline phase. Other secondary phases did not exist which is an indication that *Zn* ions were substituted by the Cobalt ions. Also, in a study on anodized *ZnO* antibacterial activity, Gilani et al. (2016) studied the structure of the films using XRD and the results revealed formation of a hexagonal wurtzite structure.

### **2.3.2 Properties and applications of *ZnO***

Huang et al. (2001) reported that the application of *ZnO* in photocatalysis is generally influenced by its large free exciton binding energy (60 meV) and direct band gap. Kong and Wang (2003) also stated that the unique properties possessed by *ZnO* like a wide band gap, photosensitivity, non-toxicity, good electrical and optical properties and its environmental stability have attracted much interest in varied applications. Other than the direct wide gap and a large exciton binding energy it also has good thermal conductivity, high electron mobility

and transparency as stated by Janotti and Van de Walle (2009). All the above properties make *ZnO* a promising material in several semiconductor applications including designing of transparent thin film transistors, heat protecting windows, light emitting diodes (LEDs), and transparent electrodes in liquid crystal displays. They are also essential in applications like antibacterial use as reported by Xie et al. (2011), gas sensors by Madhusoodanan et al. (2015), and dye sensitized solar cells by Agus et al. (2016) and photocatalysis as reported by Ong et al. (2018).

### **2.3.3 Fabrication of *ZnO* thin films and nanostructures**

Recent work by Kulkrani and Shirsa (2015) reported that several techniques have been adopted for synthesis of *ZnO* into different morphologies depending on the method of fabrication. The nanostructures that can be formed include nanorods as synthesized by Meenakshi and Sivasamy (2017), nanowires by Pung et al. (2010), tetrapods by Luo et al. (2017), nanobelts by Cao et al. (2010), nanoflowers by Xu et al. (2016), thin films by Sutanto et al. (2017) and nanoparticles by Sharma et al. (2010).

The most common fabrication techniques include: hydrothermal method, Radio Frequency (RF) and direct current (DC) magnetron sputtering, micro-emulsion, spray pyrolysis, sol-gel method, and electrochemical anodization. According to Fabbiyola et al. (2015), these methods are applicable in synthesis of pure *ZnO* nanoparticles and for *ZnO* doped with transition metals.

For hydrothermal method, Baruah and Dutta (2009) found out that hydrothermal parameters like reaction temperature and time when varied control the size and shape of *ZnO*. The limitations in this method are the difficulty to monitor the crystal growth and the high cost of

equipment such as autoclaves used. However, Suryawanshi et al. (2015) reported that *ZnO* can be synthesized using hydrothermal method acknowledging that it is one of the most promising fabrication methods for nanoscale materials where morphology, crystallinity and size of particles of the products can be controlled.

Friz and Waibel (2003) stated that sputtering techniques have low sputter rates, the materials used such as the target are expensive and there is poor use of materials but Zhang et al. (2013) studied *ZnO* thin films structural and optical properties synthesized using reactive RF magnetron sputtering and reported that high quality films could be obtained with good crystal structure, transmittance and a tunable band gap. Lee et al. (2014) also used sputtering method of deposition and found out that the optical band gap, electrical properties and the crystal structure of the films improve with increase in the sputtering power and gas pressure.

Earlier work by Salager (2000) found that microemulsion method can be used for fabrication because it is easy to prepare microemulsions and they can easily form at room temperature. This idea was seconded by Gallarate et al. (2004) who added that the microemulsions can be used since they are able to incorporate both lipophilic and hydrophilic agents. Djordjevic et al. (2004) however argued that large amounts of surfactants or co-surfactants are required in the formation of microemulsions and the high concentration of surfactants makes this method generally irritating and not the best to be used.

Patil (1999) in a study of versatility of chemical spray pyrolysis technique reported that spray pyrolysis has its final product being affected by several parameters like temperature, solute

concentration, temperature gradient, the time the film stays in the furnace, atomization technique and the carrier gases in the process. Makuku et al. (2016) however found the method simple, flexible and cost-effective. This was supported by Baghdad et al. (2017) who used spray pyrolysis to fabricate thin films of *ZnO* doped with Cobalt as they studied their magnetic and structural properties. They acknowledged that the method is simple, versatile and cheap compared to other fabrication methods.

According to Iqbal et al. (2014), sol-gel method has strength over other methods which require high processing temperature due to its low capital cost and its processing temperature is relatively low. It also has a high level of purity and uses novel materials. This was seconded by Asim et al. (2014) who stated that sol-gel method is a bridge in nanostructure synthesis especially in semiconductor metal oxides like titanium dioxide, zinc oxide and zinc titanate. They also added that this method is mostly preferred because the films formed are highly pure, have a high adhesion, are homogenous, strong and require a low processing time. More recently, Rochman and Akwalia (2017) used sol-gel method to fabricate *ZnO* nanoparticles and acknowledged its simplicity and capability to be used at lower temperatures hence less energy consumption compared to other techniques. They however state in this study that sol-gel uses a lot of chemicals and therefore the particle size formed depends on the pH of the solution where a higher pH produces bigger particles and vice versa.

#### **2.3.4 Anodization method**

This is an electrochemical process which involves forming an oxide layer on certain metal surfaces preferred for thin film production due to its cost effectiveness and the capability to

produce uniform adhesive oxide films. It also increases corrosion resistance in the metal and decorates the metal surface. Anodization is done in a simple two electrode configuration where the working electrode to be anodized (anode) along with a counter electrode (cathode) are dipped into an electrolyte. Figure 3 shows a schematic diagram for the experimental setup for anodization.



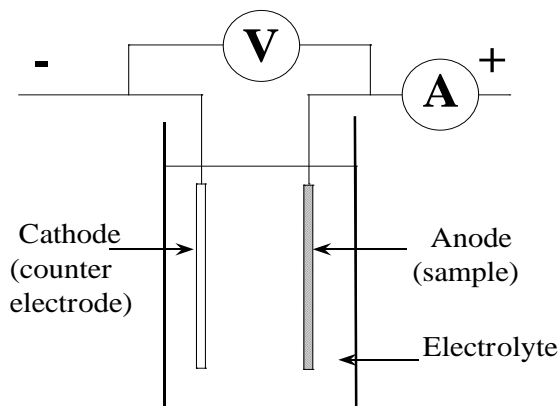


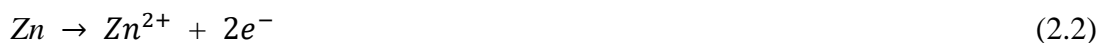
**Figure 3: Schematic diagram for the experimental setup for anodization, Nemes et al. (2011)**

Thin film formation by anodization involves applying a constant current from a power supply across the anode and the cathode which leads to oxidation and reduction reactions at the anode and cathode in that order. In the synthesis of *ZnO* thin films by anodization, Zinc is used as the working electrode and graphite or any other inert material the counter electrode. The redox reactions together with the field-driven ion diffusion result in the thin oxide layer formation on the surface of Zinc. The redox reaction equations can be expressed as:

At the cathode:



At the anode:



Fabrication of thin films by anodizing involves control of parameters like the electrolyte concentration, applied voltage, electrolyte temperature, inter-electrode spacing and anodizing

time. These parameters not only affect the nanostructure formation but also the nanostructure surface densities. The shape of the nanostructures is determined by the type of electrolyte used while the nanostructure density is influenced by the electrolyte concentration, the applied voltage and the anodizing time. Pitting may also occur at longer anodizing time, low pH of the electrolyte and high voltage.

As early as 1995, Masuda and Fukuda stated that electrochemical anodization can be widely used to design adhesive and uniform film on a metal surface increasing its corrosion wear or decorating the metal surface. Tan et al. (1998) prepared anodic coating on galvanized steel using alternating currents and found that anodic layers are porous. These layers were later reported by Imam et al. (2011) who anodized zinc to improve its surface properties. The SEM results in this study revealed that porous anodic layers formed on the zinc surface and EDX results showed presence of zinc and oxygen.

In synthesis of porous *ZnO* spheres, Zhang et al. (2011) reported that *ZnO* nanostructures such as nanoparticles and nanosheets can be obtained by anodizing zinc in different electrolytes. More recently, Voon et al. (2014) acknowledged electrochemical anodization technique as a simpler route for thin films synthesis because it is cheap, affordable and simple. This technique was used by Voon et al. (2015) who synthesized nanoporous *ZnO* by anodizing zinc in distilled water. The SEM results showed that thick *ZnO* nanostructures were formed that were distributed randomly on the surface of the zinc plate. It was also observed in this study that the morphology of the anodized plate varied with the anodizing voltage with nanoporous thin films formed between 25V and 30V. The results obtained in this study were in

consistence with those obtained by Shetty and Nanda (2012) who also anodized zinc in deionized water.

In a study of *ZnO* films antibacterial activity prepared by anodizing, Gilani et al. (2016) used 0.1M, 0.2M and 0.3M of sodium hydroxide (NaOH) and 0.1M, 0.2M and 0.5M oxalic acid ( $(\text{COOH})_2 \cdot 2\text{H}_2\text{O}$ ) electrolytes. The findings in this study revealed that a *ZnO* nano microhole array was formed in the different concentrations of NaOH but in oxalic acid nanoporous structures formed along the surface of the anodized zinc plate. It was further observed that at lower concentrations of the acid, there was an incomplete formation of the nanoparticles but at higher concentration (0.5M) a nanoparticle array was completely formed.

### **2.3.5 Semiconductor doping**

The addition of an impurity to a pure semiconductor so as to modify its properties is known as doping. The impurity can be a transition metal, non-metal or a combination of two non-metals which generate impurity levels in the band gap of the semiconductor. This deposition of the impurity onto a semiconductor may result in the impurity ions diffusing into the semiconductor structure and changing its properties including colour. This is referred to as pigmenting not doping since doping involves formation of bonds between the impurity and semiconductor atoms. Impurity levels formed in the band gap overlap with the band states and in the process the band gap is narrowed. Band gap narrowing reduces the recombination of electrons and holes enabling efficient transfer of the electrons to the conduction band. However, high impurity levels may lead to the states deep in the band gap which act as centers

of recombination for the photogenerated electrons and holes hence lowering their absorption capacity.

The band edge of *ZnO* semiconductor is in the UV region of the solar spectrum which makes it inactive in the visible light region. *ZnO* photocatalysis requires that its optical properties should be modified so as to make it absorb a broader range of the spectrum. Bahsi and Oral (2007) reported that a good tool to enhance the response to visible light in *ZnO* is by pigmenting it with transition metal cations which enhances its photocatalytic activity. Pigmenting *ZnO* with transition metal cations according to Chen et al. (2008) introduces an intermediate energy level within the *ZnO* band gap enabling it to absorb the visible light. It also reduces rate at which electron-hole recombination takes place. The researchers further state that metal ions substitute  $Zn^{2+}$  ions in the *ZnO* crystal lattice delocalizing more electrons enhancing its performance in photocatalysis. This was supported by Anandan and Miyauchi (2011) who found in their work that the best way to enhance absorption of visible light in *ZnO* is by pigmenting it with a non-metal or a transition metal.

Cobalt is a promising pigment in *ZnO* because it is able to modify its optical properties. It has a high solubility in *ZnO* due to its ionic radius and divalent state which make it applied in tuning *ZnO* optical and magnetic properties. Woo et al. (2014) acknowledges Cobalt as a preferred pigment because it creates more *Zn* vacancies in the crystal lattice of *ZnO* because of its ionic radius (0.745 Å) which is almost the same value as that of Zinc (0.74 Å). Another study on the influence of Cobalt on *ZnO* nanostructures physical properties by Zia et al.

(2014) revealed that Cobalt is a substitution pigment since it does not change the *ZnO* wurtzite structure as shown in their XRD analysis.

### **2.3.6 Post deposition treatment**

Post deposition treatment process which involves heating the as-deposited sample to a specified temperature where recrystallization can occur. This results in the removal of stacking in the individual crystal orientation and reduces the occurrence of defects in the structure. The heated films are then allowed to cool at a very slow rate so as to obtain a refined structure. Cooling is done by switching off the oven and leaving the films to cool naturally in the furnace.

This treatment makes the *ZnO* films surface rougher due to the grain sizes becoming bigger. The grain size increases with the treatment since the *ZnO* particles merge together to form bigger crystals. According to Samanta et al. (2009) as deposited *ZnO* films have higher band gap values as a result of incomplete oxidation of the films or the presence of  $Zn(OH)_2$  which is common in chemically deposited films. It also removes the  $Zn(OH)_2$  enabling complete formation of *ZnO* since the films containing  $Zn(OH)_2$  decompose into nanocrystalline *ZnO*. Reflectance also decreases on treatment due to the increase in the *ZnO* crystallite grain sizes which also leads to decrease in band gap values.

### **2.3.7 Thin film optics**

This involves the study of optical properties of a material which is generally the response of the material to an electromagnetic radiation incident on it. The radiation is partly transmitted,

partly absorbed and partly reflected by the material. The sum of the transmittance  $T(\lambda)$ , absorptance  $A(\lambda)$  and reflectance  $R(\lambda)$  is unity, Holden et al. (1997).

$$A(\lambda) + R(\lambda) + T(\lambda) = 1 \quad (2.5)$$

where  $A(\lambda) = \frac{I_A}{I_0}$ ,  $R(\lambda) = \frac{I_R}{I_0}$  and  $T(\lambda) = \frac{I_T}{I_0}$

$I_0$  is the total intensity of the radiation incident on a surface and  $I_A$ ,  $I_R$  and  $I_T$  is the intensity of light absorbed, reflected and transmitted respectively.

In absorption, the intensity  $I$  of the radiation is expressed as, Pankove (1971)

$$I(z) = I_0 e^{\frac{-2\omega k}{c}z} \quad (2.6)$$

or  $I(z) = I_0 e^{-\alpha z} \quad (2.7)$

where  $z$  is the distance in metres moved by the radiation in the absorbing medium and  $\alpha(\lambda)$  is the absorption coefficient expressed as:

$$\alpha(\lambda) = \frac{2\omega k(\lambda)}{c} \quad (2.8)$$

where  $\omega$  is the frequency of the radiation,  $c$  is the speed of light and  $k(\lambda)$  is the extinction coefficient responsible for absorption.

### 2.3.8 Characteristic matrix of thin films

Determination of optical reflectance of films is done by summing up the successive reflected beams of light given that there are two or more interfaces which will reflect the light. The film thickness for example can be deduced from the interference effects of the reflected light. It is said to be thin when the path difference between the reflected beams is smaller than the incident light coherence length and thick if the path difference is greater. In most cases, the films are considered to be thin while the substrates supporting them are seen to be thick.

Figure 4 illustrates the interaction of light with a film supported by a substrate.

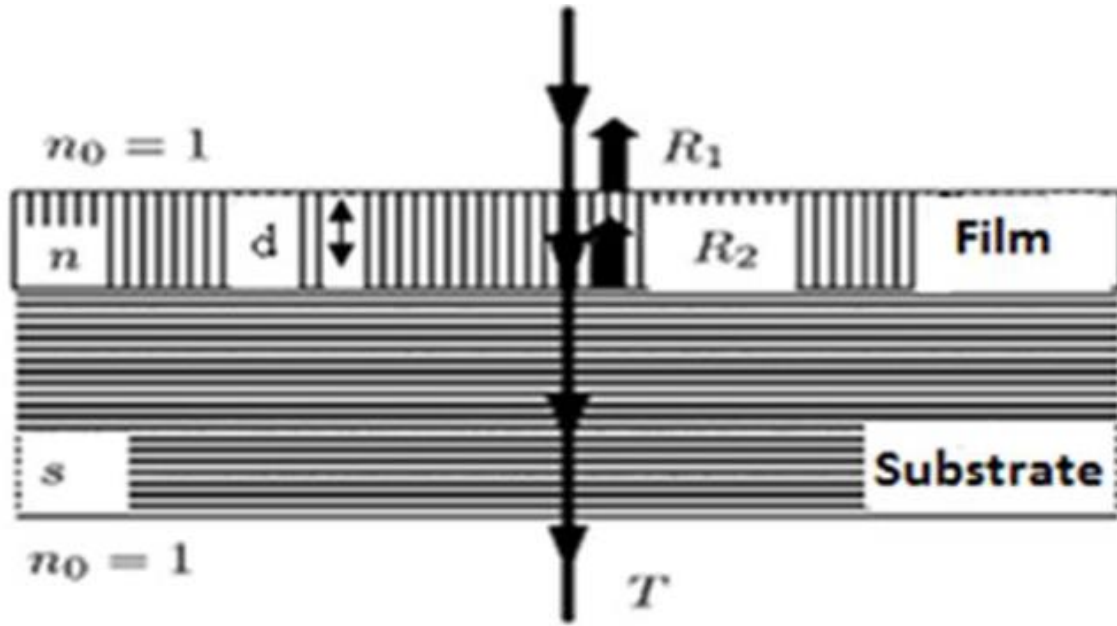


**Figure 4: A diagram illustrating the interaction of light with a film supported by a substrate, Khelladi and Sari (2013)**

If the boundary between the film and the substrate is given as  $b$  and since all the waves are moving in one direction (positive-going waves), the resultant can be obtained by summing up all the waves in the film. The resultant tangential components  $E$  and  $H$  are expressed by Macleod (1969) as:

$$E_b = E_{1b}^+ + E_{1b}^- \quad (2.9)$$

$$H_b = \eta_1 E_{1b}^+ - \eta_1 E_{1b}^- \quad (2.10)$$

Equation 2.10 is obtained from the optical admittance  $\eta$  which is expressed as:

$$\eta = \frac{H}{E}$$

Making  $E_{1b}^+$  the subject from 2.10 and substituting for  $E_{1b}^-$  from 2.9,

$$E_{1b}^+ = \frac{1}{2} \left( \frac{H_b}{\eta_1} + E_b \right) \quad (2.11)$$

$$E_{1b}^- = \frac{1}{2} \left( -\frac{H_b}{\eta_1} + E_b \right) \quad (2.12)$$

$$H_{1b}^+ = \eta_1 E_{1b}^+ = \frac{1}{2} (H_b + \eta_1 E_b) \quad (2.13)$$

$$H_{1b}^- = -\eta_1 E_{1b}^- = \frac{1}{2} (H_b - \eta_1 E_b) \quad (2.14)$$

For a point in the other boundaries with the same x and y coordinates, the resultant fields can be obtained by altering the wave phase factor so that the z coordinate can shift from zero to -d. For positive going waves, the phase factor is multiplied by  $e^{i\delta}$  and  $e^{-i\delta}$  for waves moving in the opposite direction (negative- going waves).

where 
$$\delta = (2\pi/\lambda) N d \cos\theta$$

where  $\theta$  is the direction of motion of the light wave which is obtained by Snell's law from the angle of incidence and  $N$  is the complex refractive index expressed as  $N(\omega) = n(\omega) + ik(\omega)$  and  $d$  is film thickness.

The resultant tangential components at the interface therefore become:

$$E_{1a}^+ = E_{1b}^+ e^{i\delta} = \frac{1}{2} \left( \frac{H_b}{\eta_1} + E_b \right) e^{i\delta} \quad (2.15)$$

$$E_{1a}^- = E_{1b}^- e^{i\delta} = \frac{1}{2} \left( -\frac{H_b}{\eta_1} + E_b \right) e^{-i\delta} \quad (2.16)$$

$$H_{1a}^+ = H_{1b}^+ e^{i\delta} = \frac{1}{2} (H_b + \eta_1 E_b) e^{i\delta} \quad (2.17)$$

$$H_{1a}^- = H_{1b}^- e^{-i\delta} = \frac{1}{2} (H_b - \eta_1 E_b) e^{-i\delta} \quad (2.18)$$

So that

$$\begin{aligned} E_a &= E_{1a}^+ + E_{1a}^- \\ &= E_b \left( \frac{e^{i\delta} + e^{-i\delta}}{2} \right) + H_b \left( \frac{e^{i\delta} - e^{-i\delta}}{2\eta_1} \right) \end{aligned} \quad (2.19)$$

$$= E_b \cos \delta + H_b \frac{i \sin \delta}{\eta_1} \quad (2.20)$$

$$H_a = H_{1a}^+ + H_{1a}^-$$



$$= E_b \eta_1 \left( \frac{e^{i\delta} - e^{-i\delta}}{2} \right) + H_b \left( \frac{e^{i\delta} + e^{-i\delta}}{2} \right) \quad (2.21)$$

$$= E_b i\eta_1 \sin\delta + H_b \cos\delta \quad (2.22)$$

Equations 2.20 and 2.22 can be written in matrix form as:

$$\begin{bmatrix} E_a \\ H_a \end{bmatrix} = \begin{bmatrix} \cos\delta & (i\sin\delta)/\eta_1 \\ i\eta_1 \sin\delta & \cos\delta \end{bmatrix} \begin{bmatrix} E_b \\ H_b \end{bmatrix} \quad (2.23)$$

Equation 2.23 gives the characteristic matrix of the thin film which is:

$$\begin{bmatrix} \cos\delta & (i\sin\delta)/\eta_1 \\ i\eta_1 \sin\delta & \cos\delta \end{bmatrix}$$

If there are two films on a substrate, equation 2.23 can be normalized by dividing it through by  $E_b$  so that it becomes:

$$\begin{bmatrix} E_a/E_b \\ H_a/E_b \end{bmatrix} = \begin{bmatrix} B \\ C \end{bmatrix} = \begin{bmatrix} \cos\delta & (i\sin\delta)/\eta_1 \\ i\eta_1 \sin\delta & \cos\delta \end{bmatrix} \begin{bmatrix} 1 \\ \eta_2 \end{bmatrix} \quad (2.24)$$

$B$  and  $C$  in equation 2.24 above are the front interface normalized electric and magnetic fields usually vital in determining the properties of thin films.  $\begin{bmatrix} B \\ C \end{bmatrix}$  is the characteristic matrix for the two films.

For an assembly of thin films, equation 2.23 becomes;

$$\begin{bmatrix} E_b \\ H_b \end{bmatrix} = \begin{bmatrix} \cos\delta_2 & (i\sin\delta_2)/\eta_2 \\ i\eta_2 \sin\delta_2 & \cos\delta_2 \end{bmatrix} \begin{bmatrix} E_c \\ H_c \end{bmatrix} \quad (2.25)$$

$$\begin{bmatrix} E_a \\ H_a \end{bmatrix} = \begin{bmatrix} \cos\delta_1 & (i\sin\delta_1)/\eta_1 \\ i\eta_1 \sin\delta_1 & \cos\delta_1 \end{bmatrix} \begin{bmatrix} \cos\delta_2 & (i\sin\delta_2)/\eta_2 \\ i\eta_2 \sin\delta_2 & \cos\delta_2 \end{bmatrix} \begin{bmatrix} E_c \\ H_c \end{bmatrix} \quad (2.26)$$

And the characteristic matrix is;

$$\begin{bmatrix} B \\ C \end{bmatrix} = \begin{bmatrix} \cos\delta_1 & (i\sin\delta_1)/\eta_1 \\ i\eta_1\sin\delta_1 & \cos\delta_1 \end{bmatrix} \begin{bmatrix} \cos\delta_2 & (i\sin\delta_2)/\eta_2 \\ i\eta_2\sin\delta_2 & \cos\delta_2 \end{bmatrix} \begin{bmatrix} 1 \\ \eta_3 \end{bmatrix} \quad (2.27)$$

Therefore for film with m layers, the product of the individual layer matrices given in order gives the characteristic matrix, i.e

$$\begin{bmatrix} B \\ C \end{bmatrix} = \left\{ \prod_{r=1}^m \begin{bmatrix} \cos\delta_r & (i\sin\delta_r)/\eta_r \\ i\eta_r\sin\delta_r & \cos\delta_r \end{bmatrix} \right\} \begin{bmatrix} 1 \\ \eta_m \end{bmatrix} \quad (2.28)$$

This multilayer characteristic matrix was described by Macleod (1969). For opaque substrates where there is no transmittance, the incident beam of light is accounted for by;

$$R(\lambda) = 1 - A(\lambda) \quad (2.29)$$

Where  $A(\lambda)$  is the absorbance.

$R(\lambda)$  for solar energy applications is measured from the UV to the Infrared range (300nm-2500nm) which is the solar range. Solar and terrestrial radiation is the total radiation that reaches the earth. Its intensity depends on the distance it travels in the atmosphere. Beyond the atmosphere it is said to be airmass zero (AM0) but in the atmosphere it is airmass 1.5 (AM1.5). The difference is brought about by the absorption by the atmospheric components like water vapour, ozone and carbon (IV) oxide, Duffie and Beckman (1991). Figure 5 shows the solar spectrum for airmass 1.5.

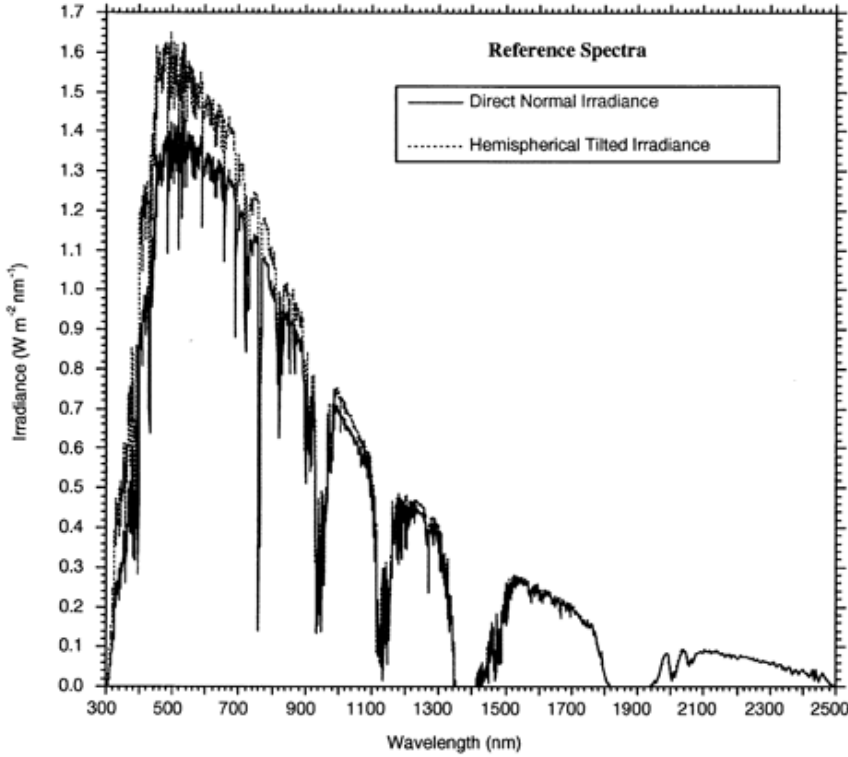


**Figure 5: Airmass 1.5 direct normal Irradiance and hemispherical tilted reflectance 37° sun facing surface, ASTM G173-03 (2012)**

The optical properties of devices are obtained by comparing them with the properties in their spectral regions which are defined by material temperatures or eye sensitivity. On earth, AM1.5 is used when determining the optical properties of devices. Integrated reflectance will be calculated later in this work by comparing the measured reflectance with AM1.5 using the equation 2.30 defined by Mwamburi and Wäckelgård (2000).

$$H_{\xi} = \frac{\int_a^b H(\lambda) \cdot \phi_{\xi}(\lambda) d\lambda}{\int_a^b \phi_{\xi}(\lambda) d\lambda} \quad (2.30)$$

Where  $\phi_{\xi}(\lambda)$  is a function of  $\xi$  and is human eye sensitivity, the earth solar irradiance or the blackbody thermal spectrum. The solar irradiance in this study at AM1.5.  $H(\lambda)$  is the measured reflectance at some range of wavelength,  $a$  and  $b$  represent 300 nm and 2500 nm respectively.

### 2.3.9 Absorption coefficient

The extent in which incident radiation of a certain wavelength penetrates a material before it is absorbed is the absorption coefficient. It is always dictated by the type of the material, the method of preparation, surface morphology and the wavelength of the incident radiation. Its study gives useful information on the electronic states at the high energy regions and atomic vibrations in the low energy regions. For thin materials, the absorption coefficient is low since they appear transparent to the radiation and they poorly absorb the radiation.

In semiconductors, the absorption coefficient has a sharp edge where radiation energy below the band gap is not energetic enough to excite an electron from the valence to the conduction band hence no light absorption. For a photon whose energy is close to the band gap energy, the absorption coefficient is low because only electrons at the edge of the valence band are excited therefore less absorption. But for a higher energy photon, not only are the electrons on the valence band edge excited but also those whose energy is near to that of the band gap. This results in more electrons interacting with the radiation consequently higher absorption.

The absorption coefficient can be obtained from the relation given by Holden et al. (1997).

$$R(\lambda) + A(\lambda) + T(\lambda) = 1 \quad (2.31)$$

According to Benno et al. (2003),

$$R(\lambda) + T(\lambda) = e^{-\alpha d} \quad (2.32)$$

When  $T(\lambda)=0$ ,

$$R(\lambda) = e^{-\alpha d} \quad (2.33)$$
$$R(\lambda) = \frac{1}{e^{\alpha d}}$$

$$e^{\alpha d} = \frac{1}{R(\lambda)} \quad (2.34)$$

$$\alpha d = \ln \left[ \frac{1}{R(\lambda)} \right] \quad (2.35)$$

$$\alpha = \frac{1}{d} \ln \left[ \frac{1}{R(\lambda)} \right] \quad (2.36)$$

In semiconductors with direct band gap, the equation that gives the absorption coefficient around the band gap is expressed as:

$$\alpha(h\nu) \propto \frac{\sqrt{h\nu - E_g}}{h\nu} \quad (2.37)$$

Therefore from this equation a plot of  $(\alpha h\nu)^2$  against  $h\nu$  gives the band gap.

In semiconductors with indirect band gap,  $\alpha$  is expressed as:

$$\alpha(h\nu) \propto \frac{(h\nu - E_g)^2}{h\nu} \quad (2.38)$$

showing that a plot of  $\sqrt{\alpha h\nu}$  against  $h\nu$  gives the band gap.

In *ZnO* nano-rod thin films structural, morphological and optical studies for biosensor applications using sol gel technique, Wahab et al. (2013) reported a decrease in absorption coefficient with increase in wavelength. They reported a sharp decrease at wavelengths corresponding to the visible region. These results were similar to those reported by Gupta and Mansingh (1996) who attributed this to surface roughness.

### 2.3.10 Optical constants, n and k

Characterization of optical constants of materials is done by their complex refractive index,  $N(\omega)$  which consists of real and imaginary terms.  $n(\omega)$  which is the real part of the refractive index indicates the phase velocity. It is the measure of how much the velocity of an incident radiation decreases in the material with respect to its speed in a vacuum. The imaginary part

on the other hand is the extinction coefficient,  $k(\omega)$  which is also referred to as the attenuation coefficient. It gives the amount of attenuation of a radiation as it propagates through the material. The complex refractive index  $N(\omega)$  is given by equation 2.35.

$$N(\omega) = n(\omega) + ik(\omega) \quad (2.39)$$

Where  $i$  is an imaginary number.

This refractive index,  $N$  relationship with the dielectric constant,  $\varepsilon$  is expressed as:

$$\varepsilon(\omega) = N^2(\omega) \quad (2.40)$$

Where the dielectric constant is defined as:

$$\varepsilon(\omega) = \varepsilon_1(\omega) + i\varepsilon_2(\omega) \quad (2.41)$$

$\varepsilon_1$  is the dielectric constant real part given as:

$$\varepsilon_1 = n^2 - k^2 \quad (2.42)$$

while  $\varepsilon_2$  is the dielectric constant imaginary part given as:

$$\varepsilon_2 = 2nk \quad (2.43)$$

From these equations the optical constants  $n$  and  $k$  can be expressed as:

$$n = \frac{1}{\sqrt{2}} \left[ \varepsilon_1 + (\varepsilon_1^2 + \varepsilon_2^2)^{\frac{1}{2}} \right]^{\frac{1}{2}} \quad (2.44)$$

$$k = \frac{1}{\sqrt{2}} \left[ -\varepsilon_1 + (\varepsilon_1^2 + \varepsilon_2^2)^{\frac{1}{2}} \right]^{\frac{1}{2}} \quad (2.45)$$

A study of zinc oxide thin films optical properties for applications in optical devices conducted by Joshi et al. (2016) found out that extinction coefficient and refractive index reduces as the wavelength is increased. Borhani and Amrollahi (2017) also studied the Effects of Cobalt Doping on  $ZnO$  Thin Films optical properties deposited by Sol–Gel Spin Coating Technique and reported that the extinction coefficient increases with Cobalt doping while the refractive index decreases.

### **2.3.11 Optical band gap**

The difference in energy expressed in electron volts (eV) between the maximum point of the valence band and the minimum point in the conduction band is the band gap. For semiconductor absorption, a rise in absorption exists at a certain value of energy which is as a result of electrons being excited from the valence to the conduction band. This minimum amount of energy that excites electrons bound in the valence band to the conduction band where they move freely within the crystal lattice is the band gap energy. These transitions of electrons in semiconductors are either direct or indirect.

For semiconductors with direct band gap, the conduction band is positioned directly above the valence band in the momentum space as illustrated in figure 6. The valence electrons can be excited directly by a photon with energy greater than that of the band gap. Electron-hole recombination easily occurs and energy is dissipated in form of light which makes direct band gap semiconductors useful for laser diodes and light emitting diodes (LEDs). Direct band semiconductors are preferred in designing thin film solar cells and photovoltaics because of their high absorption coefficient compared to semiconductors with indirect band gaps.

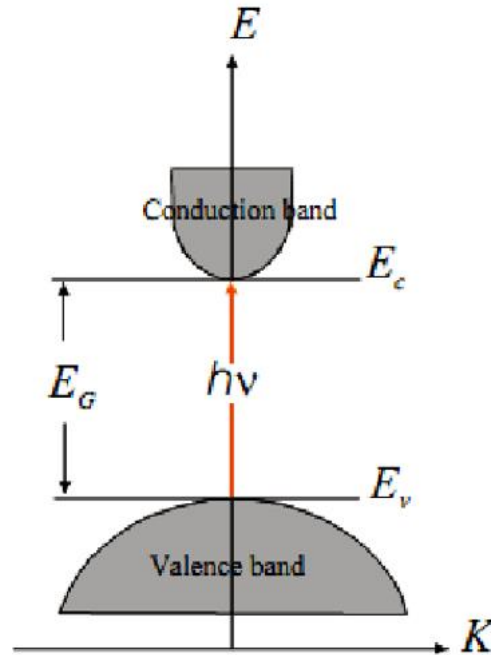


**Figure 6: Schematic diagram showing direct band gap transition, Rathod (2014)**

Semiconductors with indirect band gap have the minimum of the conduction band shifted by a difference in momentum from the maximum of the valence band. The momentum difference is represented by a  $k$ -vector. Electrons are not moved directly to the conduction band by a photon since they require some momentum source for them to reach the conduction band. In this type of semiconductors, a thicker layer is needed to absorb most of the sunlight which increases their cost. Figure 7 illustrates the indirect band gap electron transition process.



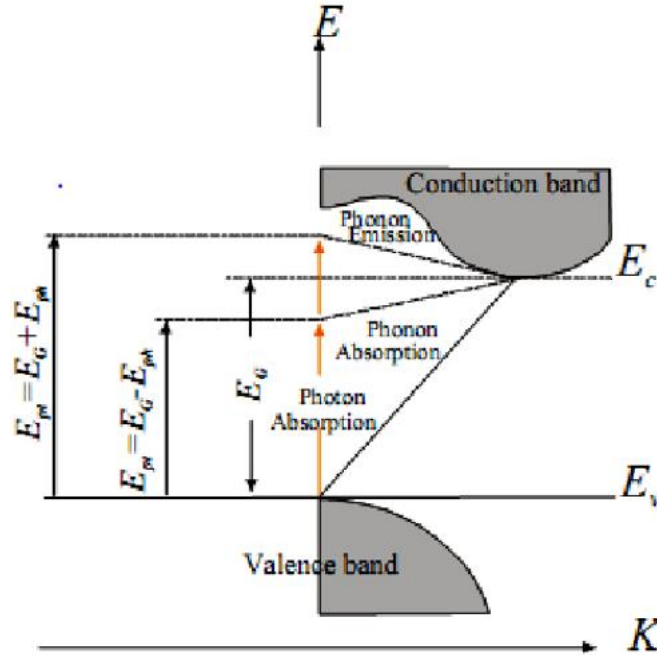


**Figure 7: Schematic diagram showing indirect band gap transitions, Rathod (2014)**

The transition of an electron from the valence to the conduction band in semiconductors is guided by the equation, Depla and Mahieu (2008):

$$(\alpha h\nu)^{1/n} = A(h\nu - E_g) \quad (2.46)$$

Where  $A$  is a constant,  $E_g$  is the band gap energy,  $\nu$  is the frequency of the radiation,  $h$  is the planck's constant and  $n$  is a number dependent on the transition type:  $n=1/2$  for direct allowed transition,  $n=3/2$  for direct forbidden transition,  $n=2$  for indirect allowed transition, and  $n=3$  for indirect forbidden transition.

### 2.3.12 Optical modelling of thin films

Knowledge on the optical constants  $n$  and  $k$  with respect to photon energy which in most cases are not available is required when investigating thin films optical properties. Fortunately, simple models of dielectric functions assist in the realistic simulation of optical spectra and

enable fitting of parameters to obtain the needed information. Some of the simulation models are Drude model for free carriers, Brendel extended oscillator model, Harmonic oscillator, KIM extended oscillator, OJL interband transition model and Tauc- Lorentz interband transition model. The choice of the model used depends on the material being studied or the spectral range and the parameters to be varied are dictated by the simulation model used.

The Lorentz and Drude models commonly used in simulation are described by the dielectric constant which can also be expressed as, Maghanga and Mwamburi (2018):

$$\varepsilon = \varepsilon_{\infty} + \chi \quad (2.47)$$

Where  $\varepsilon_{\infty}$  the dielectric constant at high frequency and  $\chi$  is susceptibility and is given as:

$$\chi = \chi_{FC} + \chi_{VE} \quad (2.48)$$

$\chi_{FC}$  and  $\chi_{VE}$  are susceptibilities for free carriers and valence electrons respectively.

The free carriers' behavior is studied by the Drude model which gives the expression:

$$\chi_{FC} = \frac{\omega_p^2}{\omega^2 + i\omega\Gamma} \quad (2.49)$$

where  $\omega$  is the frequency of the radiation,  $\Gamma$  is the damping,  $\omega_p$  is the plasma frequency of the electrons which take part in both interband and intraband transitions and depends on the number of electrons. It is expressed as:

$$\omega_p^2 = \frac{n_e q^2}{\varepsilon_0 m_e} \quad (2.50)$$

Where  $n_e$  represents the number of electrons,  $q$  is the charge of an electron and  $m_e$  is the electron mass.

The Lorentz model which considers the interband transition of the electrons investigates the behavior of the electrons bound to the nucleus. The model is governed by the expression:

$$-qE = m_e \omega_0^2 r + m_e \Gamma_D \frac{dr}{dt} + m_e \frac{d^2 r}{dt^2} \quad (2.51)$$

where  $q$  is the charge,  $E$  is the applied field,  $m_e$  is the electron mass,  $\omega_0$  is the resonance frequency,  $\Gamma_D$  is the damping parameter,  $r$  is the displacement of the electron from its equilibrium and  $t$  is the time taken to displace the electron from equilibrium.

For the nucleus bound electrons, the dielectric constant is given by the relation:

$$\varepsilon = \frac{\omega_p^2}{(\omega_0^2 - \omega^2) - i\omega\Gamma_D} \quad (2.52)$$

The plasma frequency  $\omega_p^2$  in this case is determined by the number of the electrons. It is expressed as shown in equation 2.50.

### 2.3.13 Photocatalysis

This is a reaction that occurs on semiconductor surfaces normally metal oxides and sulphides in the presence of a radiation. When photons of sufficient energy greater than the band gap energy of the semiconductor are incident on it, electrons gain kinetic energy and move from the valence to the conduction band leading to the formation of electron-hole pairs. The photogenerated electrons and holes can be useful in several photocatalysis applications. Photocatalysis is among the most researched areas currently because of its potential applications. The most commonly used semiconductor oxides in these applications are *ZnO* and *TiO<sub>2</sub>*.

Photocatalysis is classified as either homogeneous or heterogeneous where homogeneous catalysis involves use of a catalyst and reactants which are in the similar phase but heterogeneous catalysis involve unlike phases of the reactants and catalyst. Homogeneous catalysis occurs mostly in processes involving the liquid phase whereas heterogeneous occurs

in processes which use a solid phase catalyst with reactants which are either in liquid or gaseous phases. There is therefore possibility to reuse the catalyst in heterogeneous catalysis unlike in homogeneous which makes heterogeneous catalysis cheap and easy to use. Heterogeneous catalysis also has good thermal stability but poor selectivity of the active sites compared to homogeneous catalysis.

Photocatalytic process is influenced by several factors which should be considered in its application as stated by Herrmann (2005). Some of the parameters include the mass of the photocatalyst where an increase in mass enhances photocatalysis. The concentration of the photocatalyst also influences the rate at which the process takes place. This implies that for better degradation the catalyst concentration should be increased. The surface area of the reaction can be increased by reduction of the particle size of the photocatalyst. In thin films smaller particles make the film surface rougher consequently enhancing the photocatalytic process.

The wavelength or energy of the radiation determines the number of the electrons which are excited from the valence to the conduction band to be used in the photocatalytic process. The absorbed range of the radiation in terms of wavelength can be increased by altering the optical properties like narrowing the photocatalyst band gap which is done by doping or coupling it with another semiconductor. The temperature at which the reaction takes place also plays a vital role in the determination of its rate hence should also be considered, Goswami (2007).

Some of the applications of photocatalysis according to Fujishima et al. (1999) are water splitting, air purification, self-cleaning surfaces and water purification through decomposition of the organic pollutants. Air purification involves adsorption of the contaminants in air to the photocatalyst and the presence of a radiation of sufficient energy produces electrons and holes which decompose the contaminants. This process is similar to the application in self-cleaning surfaces where surfaces are coated with photocatalysts which help in decomposing any contaminants on the surface in the presence of a radiation of sufficient energy. Examples of self-cleaning surfaces are tent materials, indoor and outdoor building materials and glasses for lamps used in runway and road lighting.

Water splitting involves oxidation and reduction reactions where the photogenerated holes and electrons split water into hydrogen and oxygen. The hydrogen produced can be used as a source of clean, safe and renewable energy. The reactions for water splitting are, Maeda (2011):



In water treatment, the electrons and holes generated by light of sufficient energy in the catalyst react with oxygen and water molecules to produce superoxides ( $O_2^{\cdot-}$ ) and hydroxyl radicals ( $HO^{\cdot}$ ) which play an important part in decomposing the organic compounds in water to  $CO_2$  and  $H_2O$ . Light of energy greater than that of  $ZnO$  band gap is illuminated on it excites electrons from the valence band to the conduction band and holes are left behind in the valence band (eqn 2.55). These electrons interact with the surrounding oxygen to form superoxide radicals ( $O_2^{\cdot-}$ ) (eqn 2.57) and the holes interact with water to form hydroxyl

radicals ( $HO^*$ ) (eqn 2.56). The hydroxyl and superoxide radicals react with the organic compounds dissolved in water decomposing them to water and carbon (IV) oxide. Further reactions may take place where the hydroxyl radical formed interacts with water to produce hydrogen peroxide (eqn 2.59) which can further react with the excited electrons to produce hydroxyl radicals (eqn 2.60). The photocatalytic water treatment process therefore requires the presence of water and oxygen as summarized in equations 2.55 to 2.62, Goswami (2007):

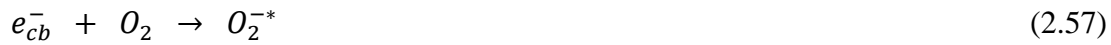
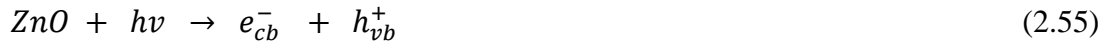
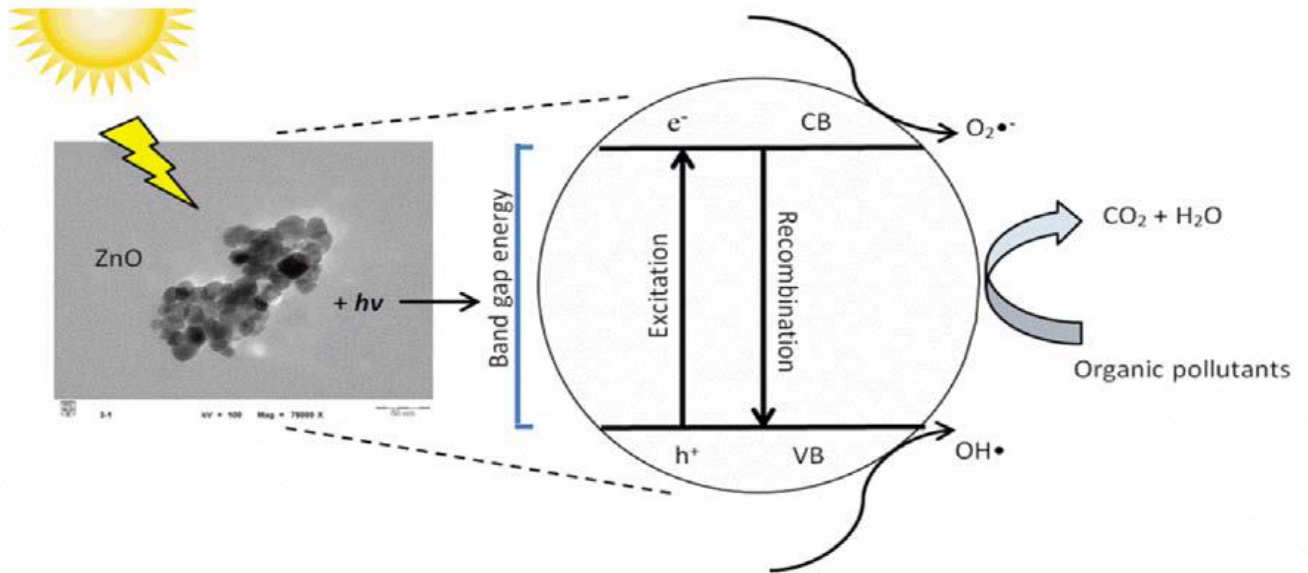


Figure 8 illustrates  $ZnO$  photocatalysis mechanism in the degradation of organic pollutants.



**Figure 8: Diagram showing *ZnO* photocatalytic mechanism, Ong et al. (2018)**

Organic pollutants degradation which is applied in water treatment process can be performed in photocatalytic reactors where the photocatalyst is placed in water or mixed with water if it is in powder form then exposed to some radiation. Some of the photocatalytic reactors that have been designed include concentrating parabolic reactor which has a glass tube placed at the focal line of a parabolic reflector. The photocatalyst can be mixed with the contaminated water and made to flow in the tube or the photocatalyst attached to the tube. The disadvantage is that this reactor utilizes only parallel and not diffuse radiation hence requires solar tracking. Also the volume of water treated by this reactor is low compared to other reactors. Its quantum efficiency according to Goswami (1995) is low and the area of the reactor tube is small hence requires high UV transmitting materials which are expensive.

A non-concentrating photocatalytic reactor unlike the concentrating utilizes both parallel and diffuse radiations, Bloss et al. (1988). It is planar and is designed such that waste water flows in through a water inlet pipe into the reactor containing the photocatalyst then leaves through a

water outlet pipe as clean water. Designing it however is expensive since the surface area required for such a reactor is large. A shallow solar pond reactor is a promising reactor in the treatment of waste water from industries and pharmaceuticals, Bloss et al. (1988). In this reactor, a photocatalyst is fixed in a shallow pond of waste water which is treated in the presence of a radiation with sufficient energy. Its disadvantage is that it is suitable only for smaller volumes of water. The other type of reactor is a thin film reactor which consists of a plate coated with a thin film of photocatalyst. When water flows over it in the presence of a radiation, it is cleaned. It is preferred over the other reactors because it utilizes both diffuse and direct radiations.

*ZnO* and  $\text{TiO}_2$  photocatalysts are activated by the Ultra Violet (UV) radiation in the solar spectrum because their band gap is wide and this limits their activity. High photocatalytic efficiency in these photocatalysts can be achieved by making them active under visible light. The techniques normally used to make them visible light active include surface modification, coupling of semiconductors, creation of oxygen vacancies and modification of the band gap by doping them with metals or non- metals.



### 2.3.14 Photocatalysis degradation kinetics

Several steps are involved in the photocatalysis degradation. In heterogeneous photocatalysis the catalyst and reactants are in phases which are not the same. This is the point of interest in water treatment because of its efficiency, reusability, simplicity and the possibility to use solar light. *ZnO* catalysis takes place on the surface and involve the 5 steps:

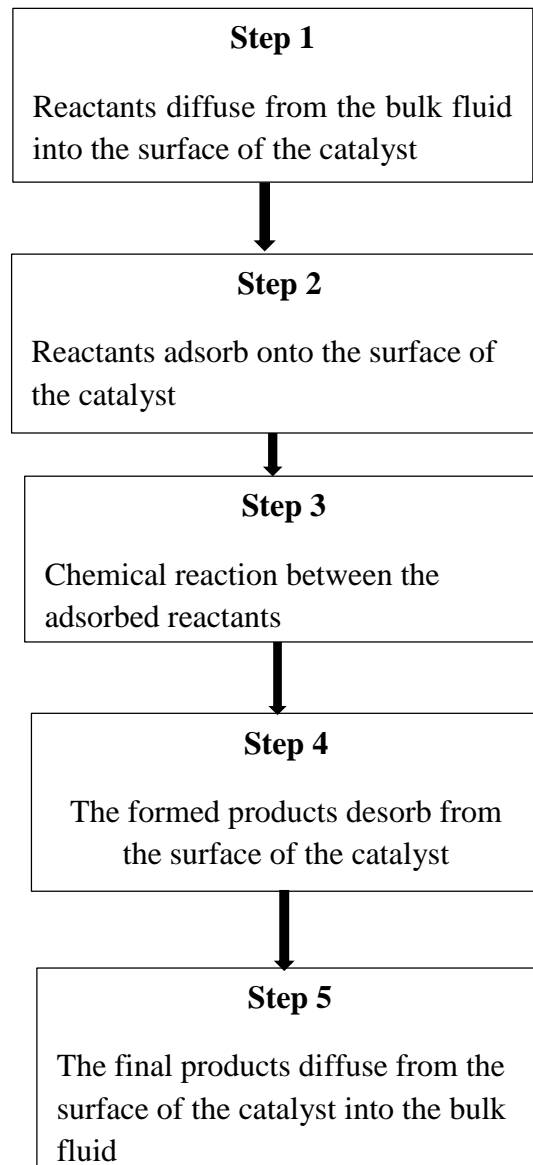


**Figure 9: Heterogeneous surface catalysis steps, Ertl (1990).**

The chemical reaction that takes place in step 3 is a concentration dependent process where a higher concentration leads to a faster reaction and a constant amount of the reactant is eliminated per unit time. The degradation kinetics in this case is first order kinetics which according to Gajbhiye (2012) the photocatalytic dye degradation follows this type of kinetics. In first order kinetics the information or data obtained is expressed in an integrated form. The change in concentration of a reactant A is expressed as:

$$\frac{-d[A]}{dt} = k[A] \quad (2.63)$$

Rearranging eqn 2.63 gives

$$\frac{d[A]}{[A]} = -kdt \quad (2.64)$$

Intergrating eqn 2.64 we obtain;

$$\ln[A] = -kt + C \quad (2.65)$$

When  $t=0$ ,  $[A] = [A_0]$

So that

$$\ln[A_0] = -K(0) + C \quad (2.66)$$

$$C = \ln[A_0] \quad (2.67)$$

This yields;

$$\ln[A] = -kt + \ln[A_0] \quad (2.68)$$

$$\ln[A] - \ln[A_0] = -kt \quad (2.69)$$

$$\ln \frac{[A]}{[A_0]} = -kt \quad (2.70)$$

Equation 2.70 is the integrated form of the first order equation which also called the rate law of first order kinetics. In this equation,  $[A]$  represents the final concentration,  $[A_0]$  is the initial

concentration,  $t$  is the time for reaction and  $k$  is the rate constant which is obtained by calculating the slope of a plot of  $\ln A/A_0$  versus time which is a straight line.

### **2.3.15 Effect of doping on photocatalysis**

Doping introduces impurity levels within the band gap of the catalyst. These levels may lie near the conduction and valence band edges hence overlapping with the band states consequently the band gap is narrowed. Heavy doping though may lead to the formation of these levels deep in the catalyst band gap. These levels act as centers where the photogenerated electrons and holes recombine hence lowering the catalyst photocatalytic activity. Increasing cobalt concentration in *ZnO* increases the oxygen vacancies and raise its absorption, Sutanto et al. (2017). Cobalt doped *ZnO* degradation of methylene blue is highest only when there is maximum oxygen vacancies indicating that there is an optimum amount of Cobalt that can enhance photocatalysis.

## **CHAPTER THREE**

### **RESEARCH DESIGN AND METHODOLOGY**

#### **3.1 Introduction**

This chapter discusses the research design, materials and the methods used in preparation, characterization of the films and study of their photocatalytic activity. The methods involve cleaning of substrates, thin film preparation by anodization and pigmentation, optical characterization and study of photocatalytic activity.

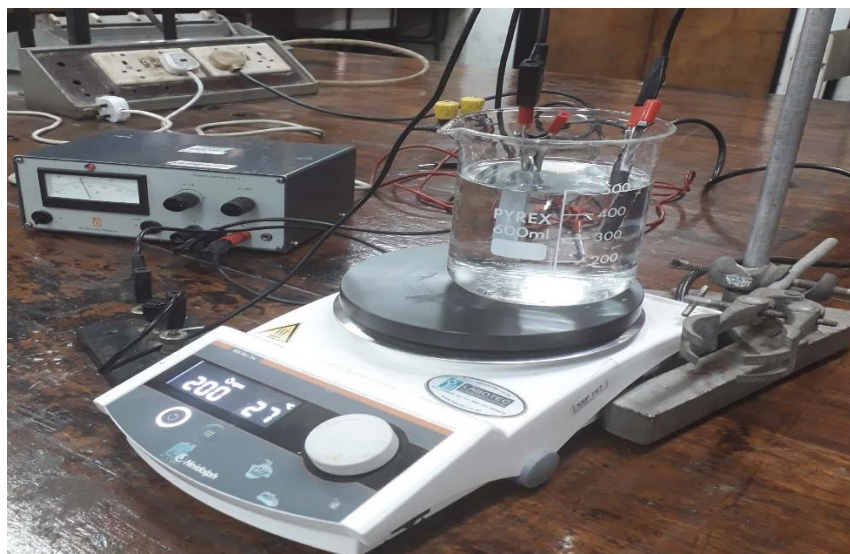
#### **3.2 Research design**

This study was experimental and was performed in the laboratory at room temperature where anodization time and the electrolyte concentration were kept constant. Cobalt deposition time was varied from 10s to 60s seconds at intervals of 10s. Data analysis involved some modelling of the data obtained experimentally. The results obtained are presented graphically and discussed.

#### **3.3 Sample preparation**

Zinc plates (about 99% pure and 2mm thick) were cut to desired size (3cm by 7cm). The surfaces were mirror-polished then cleaned by sonicating in ethanol for 5 minutes and impurities removed by rinsing in acetone. Care was taken when handling the cleaned sheets by using gloves and a pair of forceps. The cleaned sheets were dried in air then anodized at room temperature (300K) with zinc as the working electrode (anode) and graphite the counter electrode (cathode) placed 4.5cm away from each other. 0.5M magnetic stirred Oxalic acid ( $(\text{COOH})_2 \cdot 2\text{H}_2\text{O}$ ) was used as the electrolyte and anodization was done keeping the voltage constant at 10V for 60 minutes which are the conditions which gave the best films in previous

work done discussed in chapter Two. The anodized films were then rinsed in distilled water then left to dry in air. When dry, an anodic white layer formed on the Zinc metal which was specular to the eye. The plate below shows ZnO anodization experiment setup.



A plate showing the Experimental set up for anodization

Different Cobalt concentrations were incorporated into the  $ZnO$  films by electrodeposition method using 0.5M Cobalt (ii) sulphate as the Cobalt source. This was done by passing alternating current from a 20V source in the cobalt (ii) sulphate solution containing the anodized  $ZnO$  film working electrode and graphite counter electrode for 10s, 20s, 30s, 40s, 50s and 60s. Rinsing of the fabricated films was then done using distilled water. This was followed by drying of the films in air and heat treatment in a Carbolite 301 temperature controller at 523K for two hours.

The amount of Cobalt electrodeposited at different deposition times was calculated using the Faraday's law of electrochemistry expressed mathematically as, Bhattacharyya (2015):

$$m = \left(\frac{Q}{F}\right) \left(\frac{M}{z}\right) \quad (3.1)$$

where  $m$  is the mass of the substance deposited on the electrode expressed in grams,  $Q$  is the charge in coulombs passed through the substance,  $F$  is the Faraday constant (96485.33289 Cmol<sup>-1</sup>),  $M$  represents the molar mass of the substance being deposited expressed in grams mol<sup>-1</sup> and  $z$  is the valency number of the deposited substance.  $Q$  is given by the product of current passed and time in seconds ( $Q= It$ ). In this case, the substance deposited was Cobalt and the current passed was 2.18A. The molar mass of Cobalt is 58.93gmol<sup>-1</sup> and the valency is 2.

### **3.4 Instruments used in characterization of the films**

#### **3.4.1 Optical characterization**

Optical characterization was done on a PERKIN ELMER UV/VIS/NIR Lambda 19 spectrophotometer equipped with an integrating sphere. The instrument was switched on when both the sample and reference compartments were empty. Settings on the desired wavelength and the mode type whether absorbance, transmittance or reflectance were made followed by autozero so as to get the baseline measurement before the actual measurements were taken. The spectrophotometer was set to measure the reflectance of the films in the solar range 300nm <  $\lambda$  < 2500nm. The reference standard used in the measurements was barium sulphate.



A plate showing the Perkin Elmer UV/VIS/NIR Lambda 19 spectrophotometer

The UV/VIS/NIR Lambda 19 spectrophotometer is a double beam spectrophotometer which uses two beams of light: a beam that goes to the sample and a reference beam that goes to the reference standard. It is most preferred over the single beam spectrophotometer because it enables the measurement of the two beams simultaneously and its measurements are more reproducible. The reproducibility is as a result of the electronic and mechanical effects being the same on both the sample and the reference beams. Figure 10 shows the diagram of the double beam spectrophotometer with an integrating sphere.

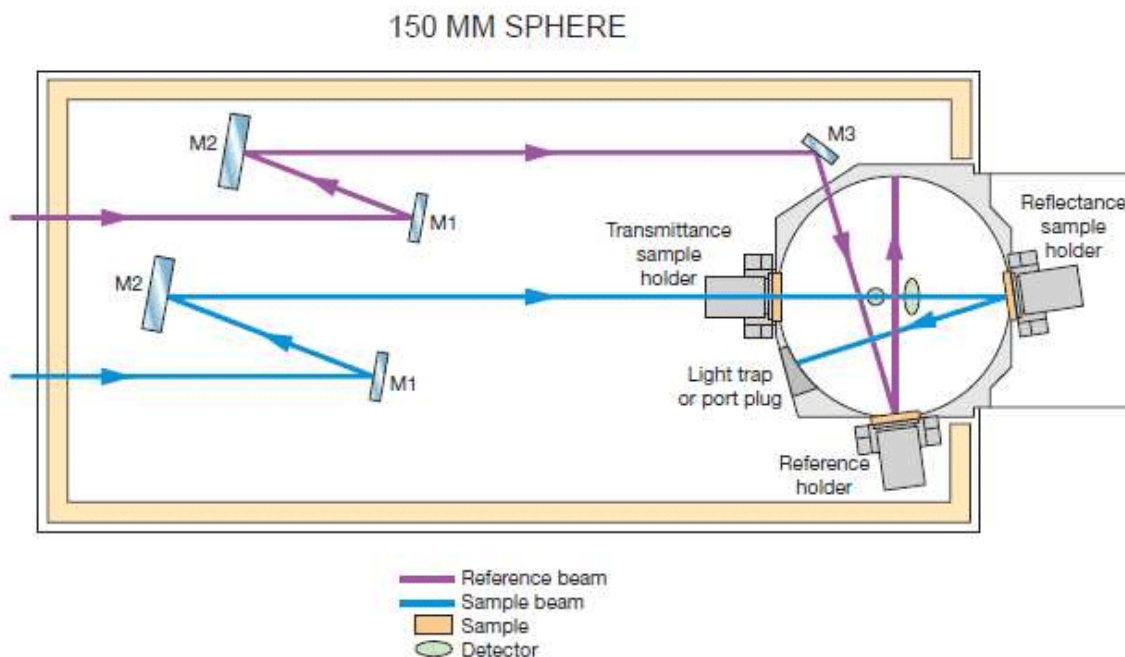


**Figure 10: Schematic diagram of the double beam spectrophotometer, Taylor (2010)**

### 3.4.2 Investigation of the photocatalytic activity of the films

The photocatalytic activity of unpigmented and Cobalt-pigmented  $ZnO$  thin films was studied for degradation of aqueous methylene blue solution which is the simulated pollutant under UV light. The system used in this study composed of a UV cabinet with a UV lamp of wavelength 366nm, 2×6W irradiation power and an Optima SP-3000nano UV-VIS spectrophotometer. The instrument was first autozeroed before using it for measurement of the sample absorbance. The sample was then dipped in 60 ml of methylene blue with 10ppm concentration in a petri dish and put in the dark for 60 minutes for adsorption-desorption balance to be reached. The petri dish and its contents were transferred into the UV cabinet and illuminated for 5 hours at ambient temperature. At intervals of 30 minutes, 1ml of the degrading solution was drawn and the absorbance directly measured at 664nm using the UV-VIS spectrophotometer. The absorbance in this case was directly proportional to the



concentration of methylene blue as revealed by a calibration curve plotted from standard methylene blue solutions of known concentrations prepared prior to the measurement. The calibration curve was used to obtain the concentration of methylene in the experiment with respect to absorbance. The rate of degradation was evaluated by comparing the methylene blue degradation without the sample, with pure *ZnO* and Cobalt pigmented *ZnO*. The pseudo-first order kinetic model according to Gajbhiye (2012) enabled quantifying of the photocatalytic activity of the samples. This model is expressed as;

$$-\ln \left( \frac{C_t}{C_0} \right) = kt \quad (3.2)$$

where  $C_t$  is the sample concentration after degradation time  $t$ ,  $C_0$  is the initial concentration of the sample after adsorption-desorption in the dark and  $k$  is the kinetic constant.

### **3.5 Data collection procedure**

At the beginning of this research work, a letter from the graduate school of Kabarak university was obtained which allowed collection and report writing. An affiliation letter was also obtained from the University Of Zambia which permitted the use of the equipment in the School of natural sciences in the institution. An application for a study permit from Zambia immigration was made but a report order was only issued for the research period.

### **3.6 Data analysis**

A commercial software called SCOUT software was used to analyze data. This software allows for simulation and analysis of different optical spectra such as absorbance, transmittance, reflectance, ellipsometry and photoluminescence. Analysis using this software is done by fitting the measured experimental data onto simulated data spectra either found

within or fed into the software. The software is a package of a variety of models including Drude, OJL, KIM and harmonic oscillator and Tauc Lorentz models which enable fitting of the spectra by varying their parameters. The choice of the model to be used in fitting of the spectra depends on the material being studied and the range of the spectrum being used. In this work, the models used were Drude, Tauc Lorentz and the harmonic oscillator.

### 3.6.1 Drude model

This model is used when the material being studied contains free charge carriers hence called the Drude model for free carriers. It is majorly used in metals and doped semiconductors where the donors or acceptors in the semiconductor set the charge carriers free. These free carriers are accelerated by radiations even with low energy and low frequencies even in the infrared region. The susceptibility of the carriers in this model is expressed as, Theiss (2000):

$$\chi_{Drude}(\tilde{\nu}) = - \frac{\Omega_p^2}{\tilde{\nu}^2 + i\tilde{\nu}\Omega_\tau} \quad (3.3)$$

And the damping constant is:

$$\Omega_p^2 = \frac{n_e^2}{\epsilon_0 m} \quad (3.4)$$

Where  $\Omega_p^2$  is the plasma frequency,  $\Omega_\tau$  is the damping constant,  $n$  is the charge carrier density,  $m$  is the effective charge mass and  $e$  is the elementary charge.

### 3.6.2 Harmonic oscillator

In the infrared region where the energy is low the vibrations which involve atomic nuclei vibrations occur. These nuclei are much heavy compared to the electrons and their resonance frequencies are in the low energy (infrared) region which depend on the strength of the bonds

between the nuclei and their masses which is useful in identifying materials hence used in analytical Chemistry to Infrared Spectroscopy.

Using SCOUT software, the harmonic oscillator model susceptibilities describe the atomic microscopic vibrations. The parameters in this model include oscillator strength, resonance position and damping. The harmonic oscillator give the expression of terms used in modelling microscopic vibrations susceptibilities as, Theiss (2000):

$$\chi_{Harmonic\ oscillator} = \frac{\Omega_p^2}{\Omega_{\tau o}^2 - \tilde{\nu}^2 - i\tilde{\nu}\Omega_{\tau}} \quad (3.5)$$

Where  $\Omega_p$  is the oscillator strength,  $\Omega_{\tau}$  is the damping and  $\Omega_{\tau o}$  is the resonance position  $\tau o$  is an index which shows that the same model also describes optical phonons ( $\tau o$ -models and lattice vibrations).

### 3.6.3 Tauc Lorentz model

Semiconductor optical absorption involves several processes in the UV-VIS-NIR because of the electronic transitions which occur between the valence and conduction bands. The interband transitions are used to parameterize the optical constants as explained by the Tauc Lorentz model which is also used in determining the dielectric constants of amorphous semiconductors for photon energies smaller than or close to the band gap. It also determines the band gap energy of the semiconductor, Rodríguez-de Marcos and Larruquert (2016). Tauc Lorentz model combines the Lorentz oscillator with Tauc's model of the density of states. According to Tauc's approach, the density of states in the valence and conduction bands is parabolic and the wave vector  $\mathbf{K}$  is not a good quantum number. The absorption coefficient is expressed as, Angulo (2016):

$$\alpha_{Tauc} = \frac{\alpha_0}{\hbar\omega} \iint D_C(E_C)D_V(E_V)\delta(E_C - E_V - \hbar\omega)dE_VdE_C \quad (3.6)$$

Where  $D_C(E_C)$  and  $D_V(E_V)$  are the densities of states for conduction and valence bands respectively,  $E_C$  and  $E_V$  are the conduction and valence band edges,  $\hbar\omega$  is the photon energy and  $\alpha_0$  is the optical absorption coefficient.

Using Tauc's model framework to solve the integral, the absorption coefficient will be:

$$\alpha_{Tauc} = M_{Tauc}^2 \frac{(\hbar\omega - E_{Tauc})^2}{\hbar\omega} \quad (3.7)$$

Where  $M_{Tauc}^2$  is a constant and  $E_{Tauc}$  is the Tauc-gap.

The graph of  $\sqrt{\alpha\hbar\omega}$  versus photon energy and is from these equations gives a straight line.  $E_{Tauc}$  is the energy axes intercept and gives the value of the band gap.

In the SCOUT software, Tauc Lorentz model has four parameters which must be entered using wavenumber units which are: resonance frequency, strength, damping and gap. The model gives the expression for the susceptibility as:

$$\chi_j(\omega) = \frac{1}{\omega} \frac{S^2 \omega_0 \omega_\tau (\omega - \omega_{Gap})^2}{(\omega^2 - \omega_0^2)^2 + \omega^2 \omega_\tau^2} \Theta(\omega - \omega_{Gap}) \quad (3.8)$$

Where  $S$  is the strength,  $\omega_\tau$  is the damping constant,  $\omega_0$  is the resonance frequency and  $\omega_{Gap}$  is the band gap energy.

In this study, the models discussed above enabled fitting of the experimental reflectance data to the simulated data in the (0.4 -1 $\mu$ m) range, Theiss (2000) which made it possible for thickness of the films and optical constants to be determined. This set of data was exported from the software once an acceptable fit of the experimental and simulated spectra was obtained. The data exported included the wavelength, extinction coefficient, real and imaginary parts of the dielectric constants and refractive index. The absorption coefficient was calculated from the thickness of the films obtained and reflectance then plotted against the

radiation wavelength. The extinction coefficient and refractive index were plotted directly against the corresponding wavelength and presented graphically.

For optical band gap determination, the absorption coefficient obtained from the SCOUT software was used to find  $(\alpha h\nu)^2$  and energy of radiation ( $h\nu$ ) was calculated. The data obtained was used to plot the Tauc's plot of  $(\alpha h\nu)^2$  against energy. This plot gave a curve whose linear extension revealed the band gap values of the films.

## **CHAPTER FOUR**

### **DATA ANALYSIS, PRESENTATION AND DISCUSSION**

#### **4.1 Introduction**

This chapter gives the findings, interpretations and discussions of the research work. *ZnO* films fabrication by anodization is presented. The rate of incorporation of Cobalt in the *ZnO* films, their interaction with radiation and the photocatalytic performance of both pure and Cobalt-pigmented *ZnO* thin films are also presented. The powerful tool of interpreting optical reflectance spectra by simulation of experimental data and fitting onto simulated data by adjusting the model parameters was put to use. Once a satisfactory fit was achieved, the required information could be obtained. This analysis was carried out in the range  $300 \leq \lambda \leq 2500$  nm.

#### **4.2 Results and discussion of the study**

##### **4.2.1 Deposition of *ZnO* films**

*ZnO* films were successfully fabricated on the Zinc substrate where a white film formed on its surface. *ZnO* is white in colour. The formation of the white film on Zinc electrode surface confirmed formation of *ZnO* film which resulted from passing of a constant current from the power supply. Consequently, redox reactions at the anode and cathode led to the oxide forming since  $Zn(OH)_2$  on the Zinc substrate further dissociated to *ZnO*. The average film thickness of the fabricated pure *ZnO* sample in this study was modelled using SCOUT software where the obtained experimental spectra was fitted to the simulated spectra within the software as illustrated in figure 11. The average thickness of the fabricated films was 110nm.

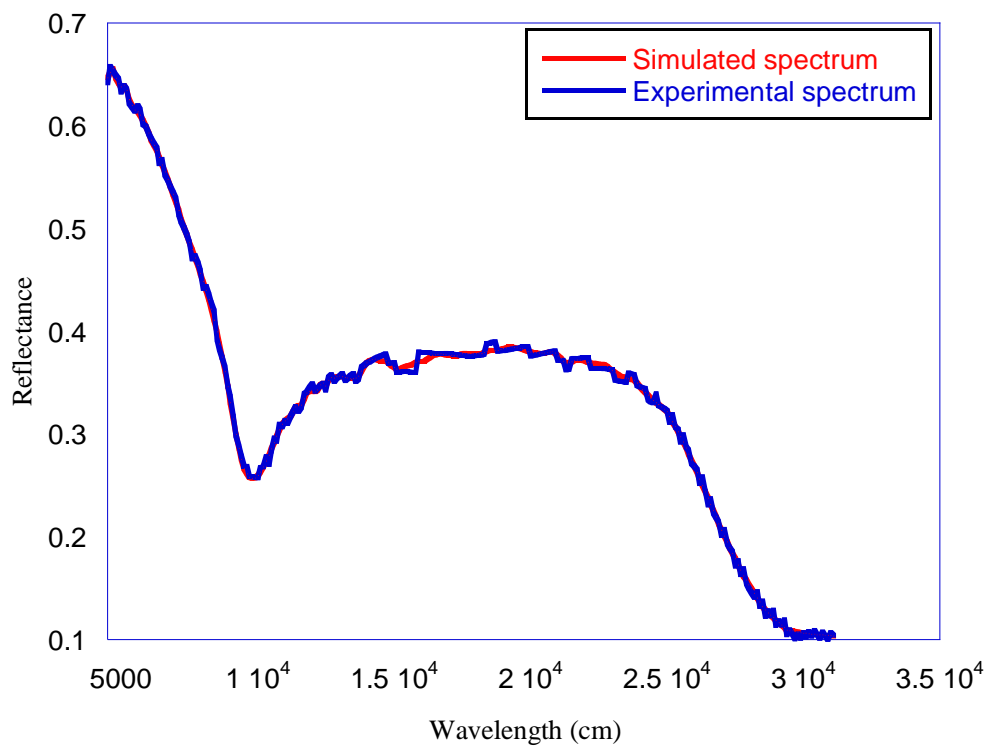


**Figure 11: An illustration of fitting of the experimental to simulated spectra using the SCOUT software**

#### 4.2.2 Cobalt pigmentation in the *ZnO* films

Cobalt was electrodeposited in the *ZnO* films at varying deposition time. Figure 12 displays variation in the amount of Cobalt electrodeposited in *ZnO* with the deposition time.

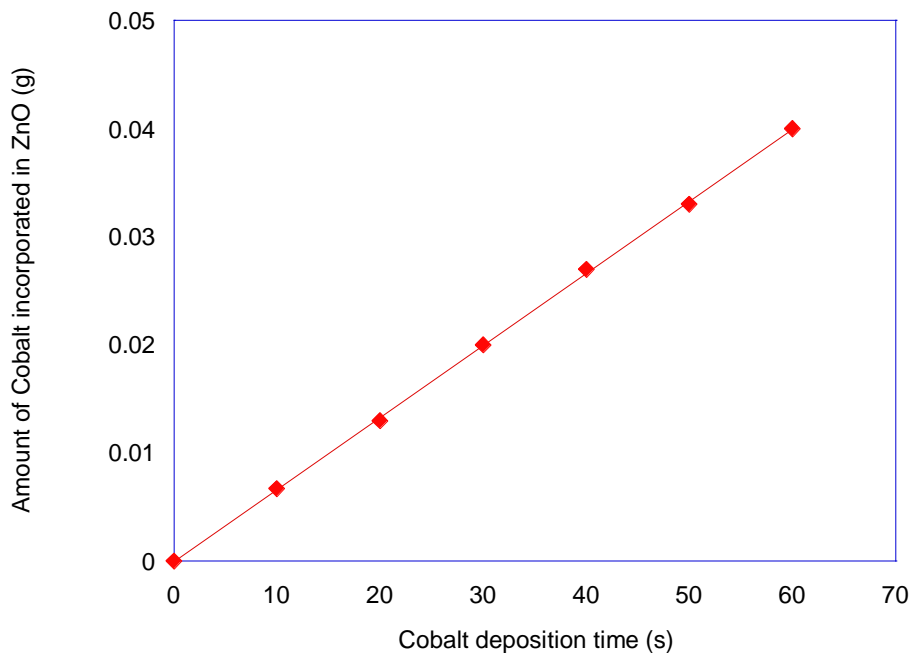


**Figure 12: Graph showing the variation of calculated amounts of Cobalt deposited (g) and the deposition time (s)**

The data used to plot the graph in figure 12 was obtained using the relation given by Faraday's law which gives the quantity of the deposited substance with respect to deposition time and the current passed. As observed in figure 12, increasing the Cobalt deposition time resulted in higher quantities of Cobalt deposited in the *ZnO* films indicating direct proportionality. The rate of deposition which is the slope of the graph was found to be 0.0007 g/s.

Although there was an increase in the amount of Cobalt deposited on *ZnO* when the time at which Cobalt was deposited increased, the change in film thickness was not much since it



increased from 108.3nm to 110.0nm for ZnO and ZnO:Co 60s respectively. This may be due to Cobalt being incorporated into the *ZnO* film leading to less change film thickness. Optical properties were however observed to be affected by the amounts of Cobalt deposited. This may be due to the substitution of the Zinc ions by the Cobalt ions in the *ZnO* crystal structure.

White *ZnO* films were observed to darken upon introduction of Cobalt and this became more pronounced as the deposition time was increased. Darkening of the *ZnO* films may be attributed to Cobalt pigmentation in the *ZnO* films. The films became darker as the Cobalt deposition time increased. The darkening observed in the films was an indication of enhancement in the absorption by the films as Cobalt is incorporated in the films since reflectance in darker or dull surfaces is lower than shiny or polished surfaces.

### **4.2.3 Optical characterization of the films**

#### **4.2.3.1 Reflectance spectra**

Figure 13 shows the spectra for the measured reflectance for the polished Zinc metal before anodization and the as-deposited *ZnO* film.

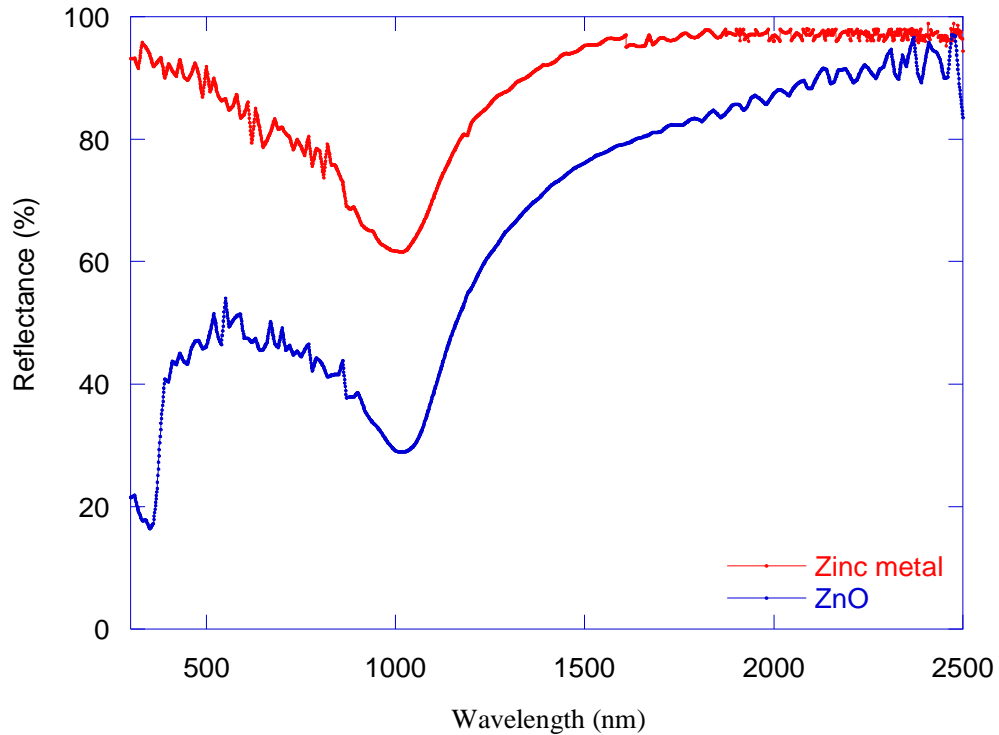


**Figure 13: Measured reflectance as a function of wavelength for polished Zinc metal and as-deposited *ZnO* film**

Polished Zinc metal has a high reflectance more than 60% in the whole range from 300nm to 2500nm because of its shiny surface. The fabricated *ZnO* thin films had a relatively lower reflectance although its reflectance was still regarded to be high. This may be as a result of *ZnO* specular white colour. It could also be due to effects of the shiny Zinc substrate on which the thin *ZnO* films were fabricated. A decrease in the reflectance in both spectra was observed at about 1100nm. This deep is due to Zinc metal parallel band absorption as seen in the data presented by the handbook of optical constants, Palik (1998).

Unlike the Zinc metal spectrum, a sharp decrease in *ZnO* reflectance spectra was observed in the UV region at about 348nm which was related to its absorption edge. This is in good agreement with the fact that *ZnO* has high absorption in the UV than the visible region because of its wide band gap. The rise in reflectance for wavelengths greater than 1000nm is explained by the classical Drude theory which assumes that a free electron gas moves between the ions in the crystal lattice. This high electron concentration forms plasma hence high reflectance. The Drude theory fails at low film deposition temperatures, low wavelengths or high frequencies of the solar spectrum.

The visible region of the spectrum was seen to have some oscillations which may have resulted from transitions of the electrons which take place between the valence and the conduction band as the radiation energy increases towards the band gap energy. This could also be due to multiple reflections that result in the interference of the light which is reflected from both the film and the substrate which have different refractive indices.

Figure 14 shows the reflectance spectra of *ZnO* films with varying Cobalt concentrations.

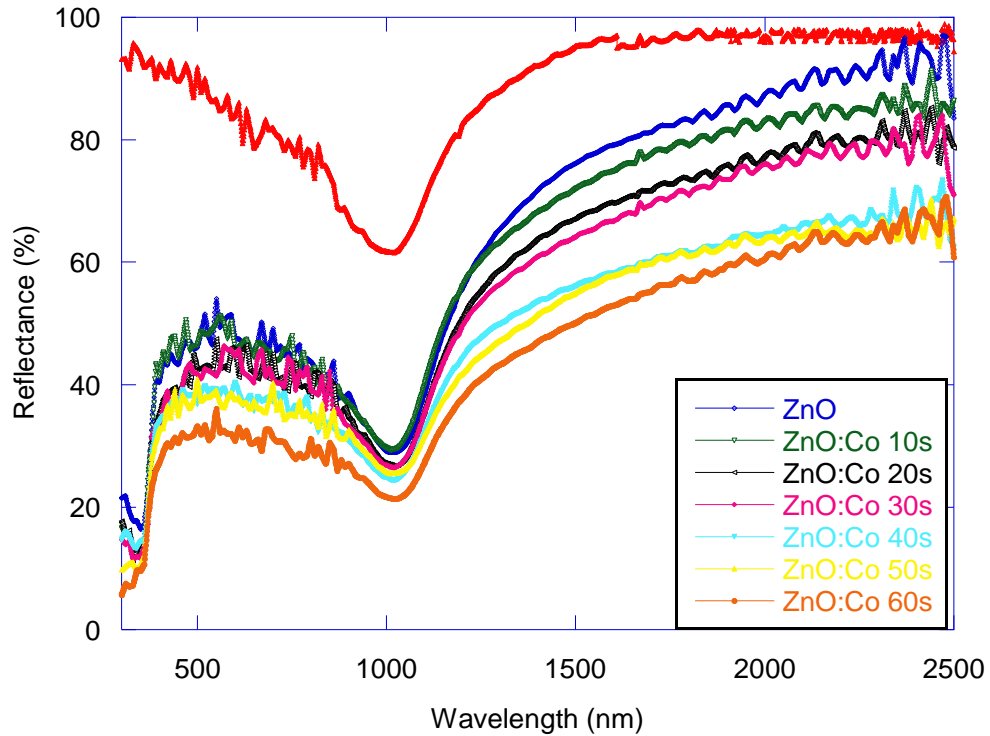


**Figure 14: Measured reflectance for Zinc and the *ZnO* films with different Cobalt concentrations**

As seen in the figure, Cobalt pigmenting affects reflectance since more Cobalt deposited in the films lowers the reflectance. This may be attributed to the darkening of the films as the Cobalt concentration was increased as discussed in section 4.2.2. It may also be due to the *ZnO* films becoming rough as Cobalt is deposited as stated by Yousif et al. (2012). The more the Cobalt concentration, the rougher the films hence the decrease in the amount of light reflected. A decrease in reflectance implies more light absorption (absorbance).

The change in reflectance in the films was quantified by calculating their integrated (average) reflectance. Figure 15 shows variation of integrated reflectance with Cobalt concentration.

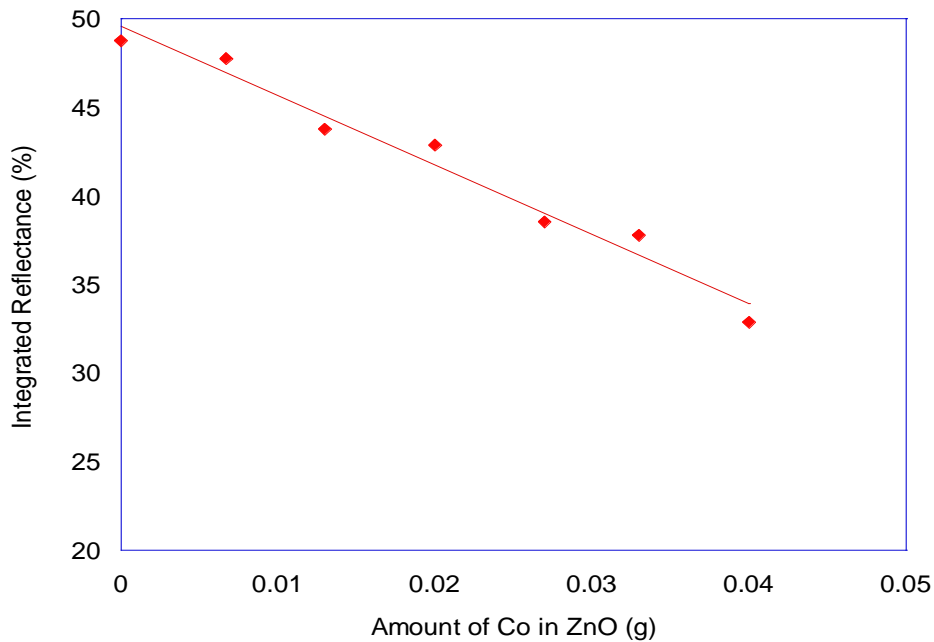


**Figure 15: Change in integrated reflectance with increase in Cobalt concentration**

Figure 15 confirms the observation made in the reflectance spectra presented in figure 14 showing a decrease in reflectance when Cobalt was introduced into *ZnO* which was attributed to *ZnO* surface roughness as the Cobalt concentration was increased. This may have resulted in diffuse reflection that captured the reflected light and enhanced its absorption. The roughness may also have led to scattering of light at the surface due to the decrease in the grain size of the *ZnO* crystals resulting from the incorporation of Cobalt. The decrease in reflectance with increase in Cobalt concentration may be associated to more light scattering due to the film roughness.

There was a shift towards longer wavelengths (Red shift) in the absorption edge which was observed in all the prepared films. This shift according to Jain et al. (2006) results from band gap narrowing in the films when pigmented with a transition metal. Figure 16 shows the shift in some sampled films for clarity purposes.

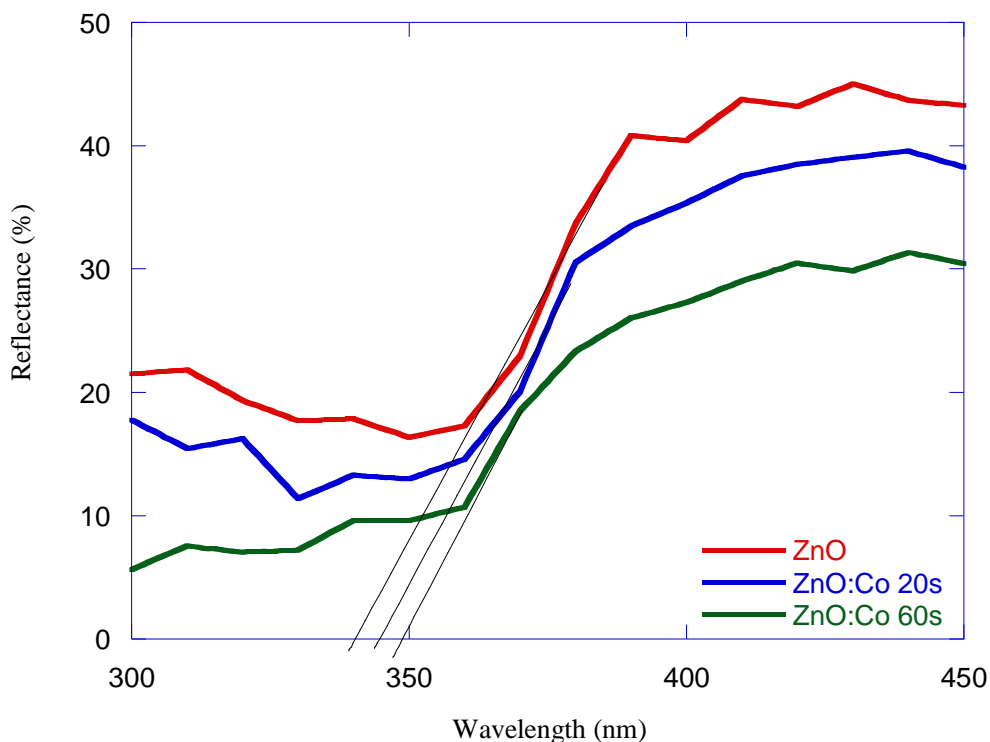


**Figure 16: Effect of Cobalt pigmenting on the *ZnO* absorption edge for some sampled films**

The shift in the absorption edge towards longer wavelengths indicated increase in absorption. It also showed that there may have been a change in the *ZnO* electronic band structure which may have resulted from the Zinc ions being substituted by the Cobalt ions. This resulted in the

Fermi level moving up towards the conduction band hence increased absorption. The shift as observed in figure 16 was seen to depend on the Cobalt concentration where a larger shift from the initial edge was observed in the films with higher Cobalt concentration. The films with higher Cobalt concentrations therefore may be more absorbing which supports the fact that heavily pigmented films became darker and had a more reduced reflectance.

#### 4.2.3.2 Absorption coefficient

Figure 17 shows the variation of the absorption coefficient with wavelength.

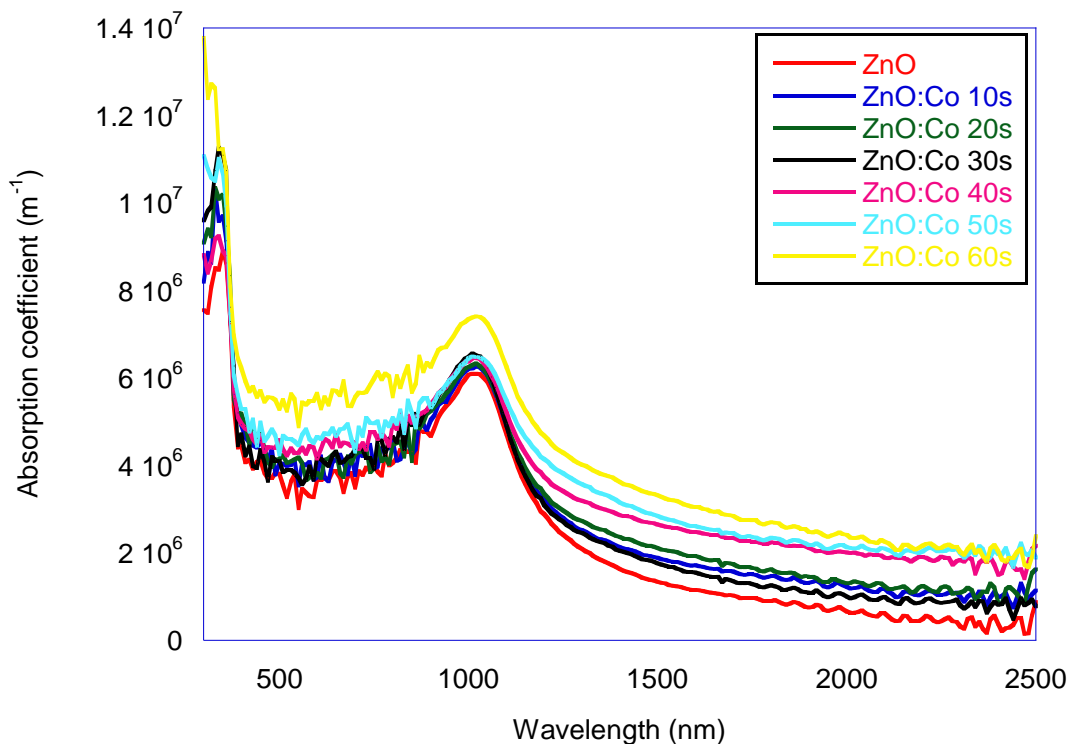


**Figure 17: Absorption coefficient ( $\text{m}^{-1}$ ) versus wavelength (nm)**

The absorption coefficient data used to plot figure 17 was determined from the relation given in equation 2.36 expressed as:

$$\alpha = \frac{1}{d} \ln \left[ \frac{1}{R(\lambda)} \right]$$

As observed in the figure, at shorter wavelengths where the films absorb the absorption coefficient is greater than  $10^6 \text{ m}^{-1}$  which according to Bakr et al. (2015) shows a high probability for direct transition. A sudden increase in the absorption coefficient was also observed at shorter wavelengths about 348nm which correspond to the absorption edge. The absorption coefficient was however low at longer wavelengths. A high absorption coefficient of a material suggest that high quantities of light being absorbed by the material. This clearly indicates that the radiation was absorbed at shorter wavelengths than at higher wavelengths.

Cobalt pigmentation was also observed to affect the absorption coefficient since an increase in the Cobalt concentration increased the absorption coefficient. This may be as a result of the decrease in the reflectance of the films as Cobalt concentration was increased. According to Bakr et al. (2015) the pigment content in a film affects its absorption. The peak observed at about 1000nm shows absorption due to the Zinc substrate which resulted from interband transitions within the substrate. Interband transition in Zinc metal occurs at about 1000nm, Palik (1998).

#### **4.2.3.3 Optical constants**

The refractive index,  $n$ , and the extinction coefficient,  $k$ , for the prepared films are presented in figure 18 (a) and (b) respectively.



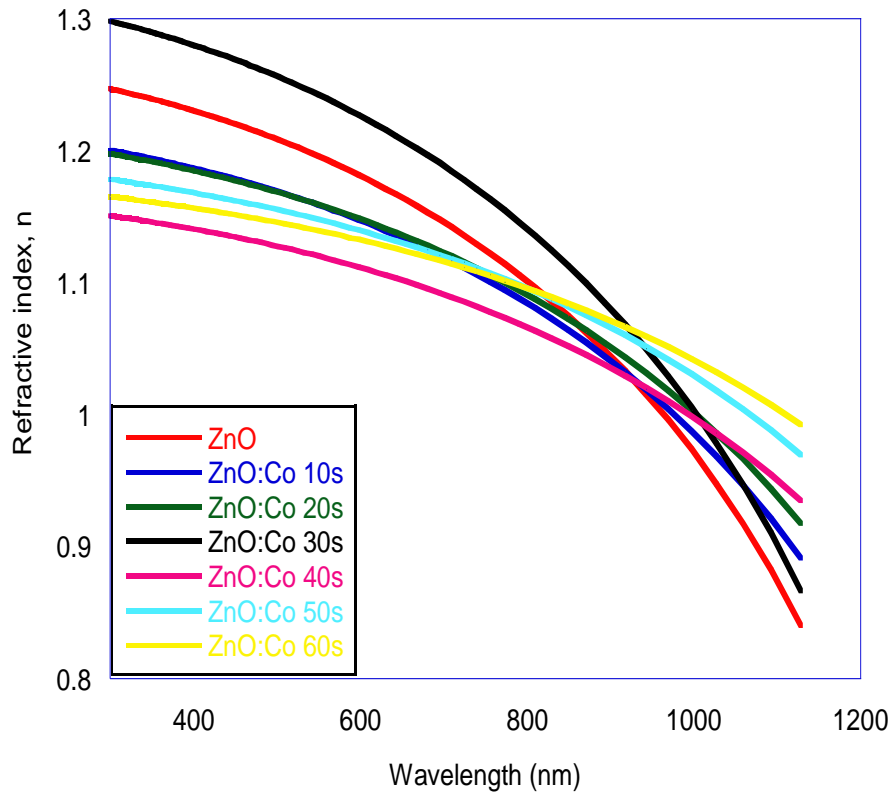


**Figure 18 (a): Refractive index,  $n$  of the prepared films as a function of wavelength**

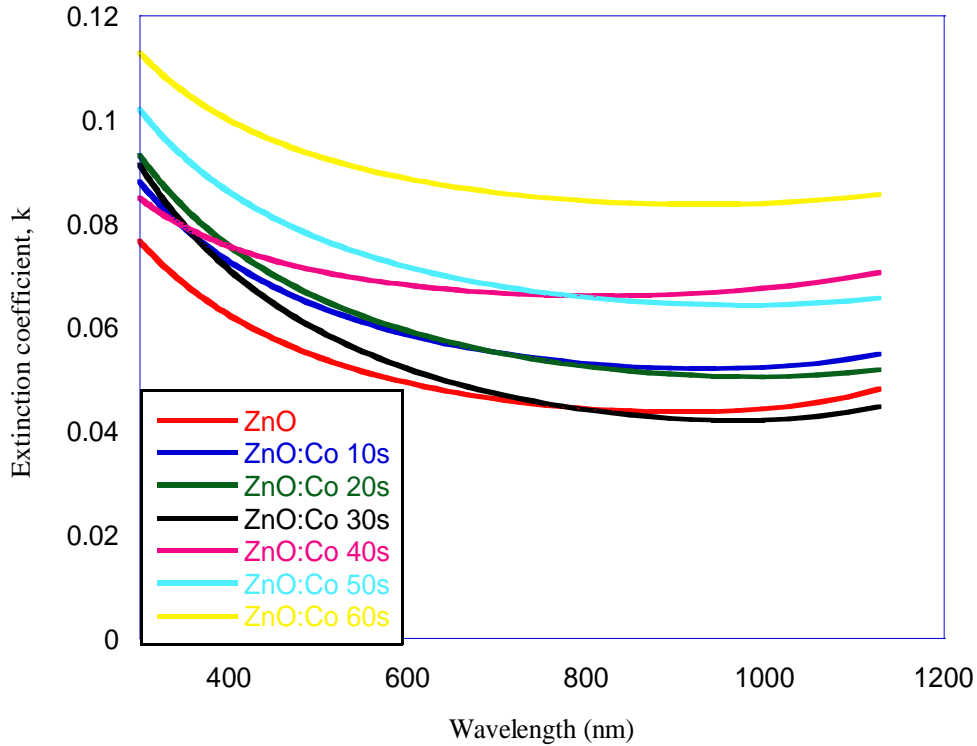


**Figure 18 (b): Extinction coefficient,  $k$  of the prepared films as a function of wavelength**

The refractive index of the deposited films was lower than that of glass (1.5) and that of  $ZnO$  fabricated using other methods which may be due to a low density of the  $ZnO$  film formed on the substrate which may not be compact but has voids within its structure. Zinc metal has low refractive index which is about 1.04, Polyanskiy (2019). The low refractive index of the  $ZnO$  films may be attributed to the zinc substrate which is exposed at the voids. The films may also be thin and appear to be transparent to the radiation. Cobalt pigmentation was observed to decrease the refractive index which may be due to  $ZnO$  crystal size reducing as the cobalt concentration increases. The increase observed for  $ZnO:Co$  30s may be due to film disorder or lattice distortion.

In figure 18(b), it is observed that an increase in wavelength leads to a decline in the extinction coefficient. The extinction coefficient however increases with pigment concentration which may be as a result of optical loss due to increase in surface scattering.

#### 4.2.3.4 Optical band gap

The band gap of *ZnO* semiconductor is direct therefore it can be obtained from a plot of  $(\alpha h\nu)^2$  versus energy in eV. Figure 19 shows the graph used to obtain the band gaps of the prepared films.

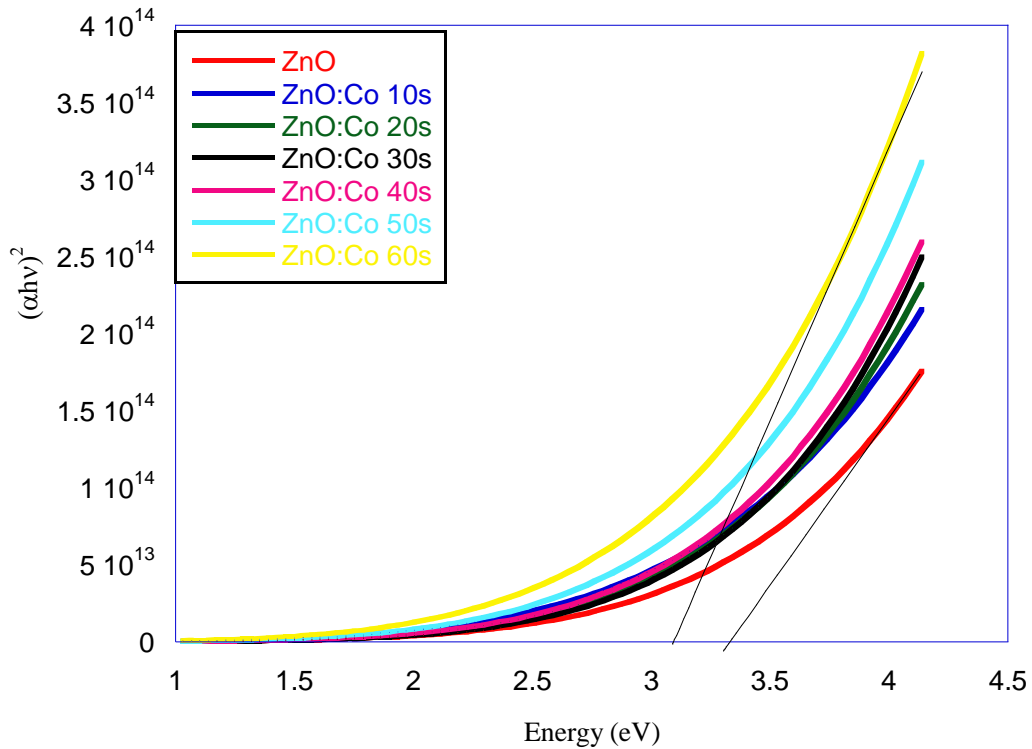


Figure 19: Graph showing the band gap analysis of the fabricated films

The optical band gaps for the prepared films obtained from the plot ranged from 3.34 eV to 3.10eV. The fabricated pure *ZnO* films had a band gap of 3.34 eV which is similar to the preceding work done by Yildirim et al. (2016) who also found 3.34 eV. A gradual decrease was observed as Cobalt was introduced into the *ZnO* films in different amounts. This decrease is associated with the red shift observed in the reflectance spectra.

A gradual decrease in *ZnO* optical band gap as Cobalt pigmentation increases was also reported by Kao et al. (2011), Sutanto et al. (2017) and Borhani and Amrollahi (2017) who attributed the decrease to sp-d exchange interactions between the d electrons of Cobalt and *ZnO* conduction band electrons once the Cobalt ions substitute the Zinc ions in the crystal lattice. High Cobalt concentration also led to the wavefunctions of the electrons in the Cobalt atoms overlapping as the Cobalt density increases. Consequently an energy band was formed by the overlapping forces which explains the reduction in the band gap.

Post deposition heat treatment was observed to have an influence on the films band gap values since the values of the gap in the as-deposited films were from 3.40 eV, 3.37 eV, 3.36 eV, 3.35 eV, 3.32 eV, 3.31 eV, 3.20 eV for pure ZnO to ZnO:Co 60s in that order. These values were higher than those obtained after the heat treatment shown in figure 19 which ranged from 3.34 eV to 3.10eV. The decrease in band gap on annealing *ZnO* thin films doped with transition metal was also reported by Mathew et al. (2015). This may be as a consequence of the Cobalt ions on the surface of the as-deposited films which had not diffused into the *ZnO* crystal lattice. Heat treatment however made some Cobalt ions to diffuse into the lattice,

removed the defects and allowed recrystallization to occur hence enhanced the crystallinity and the grain sizes.

It also may have led to the decomposition of  $Zn(OH)_2$  compound which could have been present in the as-deposited films and made them to have higher band gaps. The reduction in band gap in most cases is linked with the annealing temperature, presence and amount of pigment, thickness of the films, presence of defects and the size of the sample, Yildirim et al. (2016). In this case it was attributed to the presence of defects and amount of pigment since the temperature, sample size and film thickness were the same for all the films.

#### **4.2.4 Pure and Cobalt pigmented $ZnO$ photocatalytic degradation of methylene blue**

Fading of methylene blue solution was observed in the course of the experiment implying that degradation was taking place hence an effect in its concentration. Fading of the color led to a decrease in its absorbance as measured by the spectrophotometer. Its transmittance was observed to increase since it became clearer as it was degraded. The methylene blue concentration was not measured but the absorbance measured was used to obtain the corresponding values of methylene blue concentration using the calibration curve shown in figure 20.

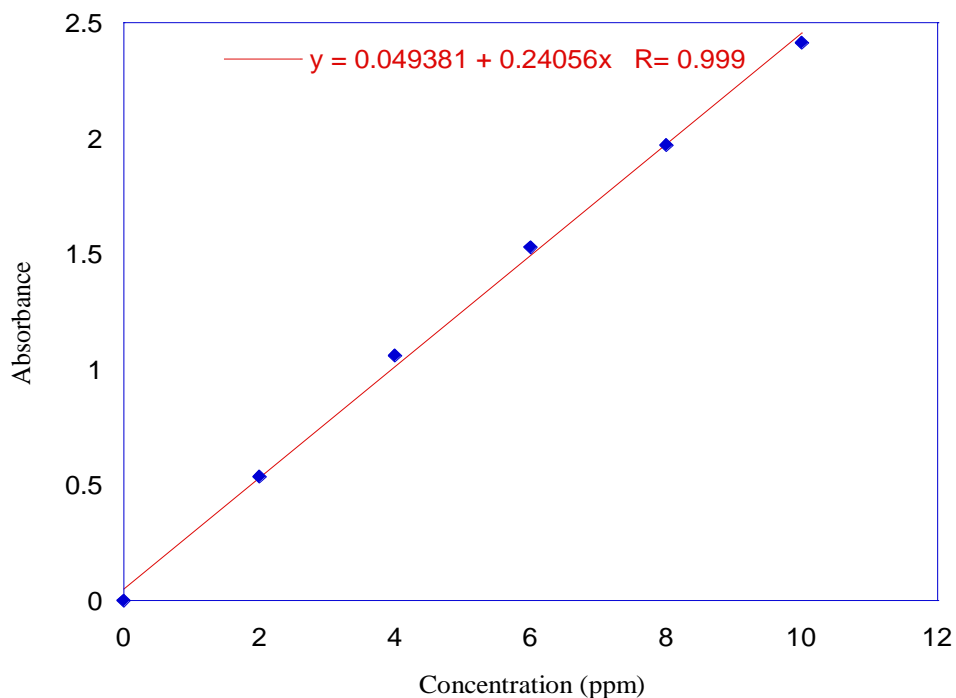


**Figure 20: Methylene blue calibration curve**

The radiation induced photocatalytic degradation of methylene blue follows the pseudo first order kinetics which involves the presentation of raw data as integral data. Figure 21 shows the performance of the pure and Cobalt pigmented *ZnO* films. The photocatalytic performance of the films was studied in comparison to that of methylene blue degradation without the catalyst.

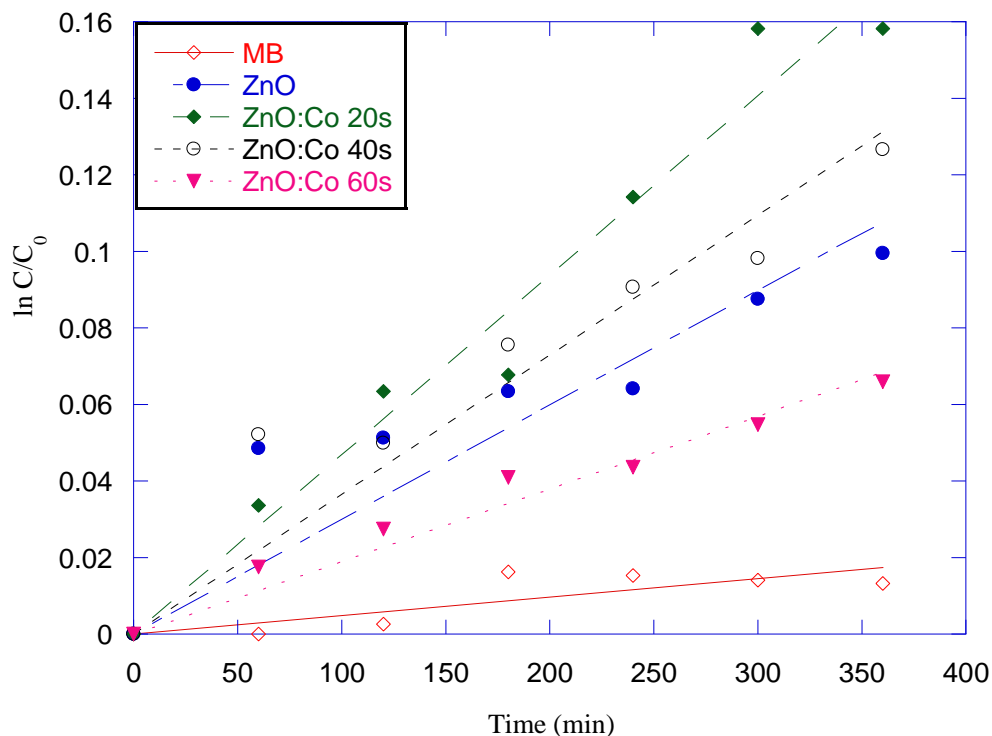


**Figure 21: A graph of  $\ln (C/C_0)$  versus time in minutes for sampled films**

As observed in the figure, the rate at which methylene blue with catalyst was degraded was faster than that without the catalyst. Also, Cobalt pigmentation increased the degradation rate. This may be attributed to the reduction in the optical band gap resulting from the red shift in the reflectance spectra which allowed more electrons to gain kinetic energy and move to the conduction band and take part in the degradation process. Cobalt pigmentation also increased the absorption coefficient implying that more radiation was absorbed which excited more electrons to the conduction band.

Heavy Cobalt pigmentation however lowered the methylene blue degradation rate. This may be due to the fact that excess metal pigment covered the active sites of the  $ZnO$  catalyst lowering its activity or the generation of the impurity levels deep in  $ZnO$  band gap which acted as centers for recombination for the photogenerated electrons. The slope of the plot in figure 21 was used to determine the rate constant,  $k$  which enabled quantification of the activity of the prepared samples. Figure 22 shows how the rate constant varied with Cobalt concentration.

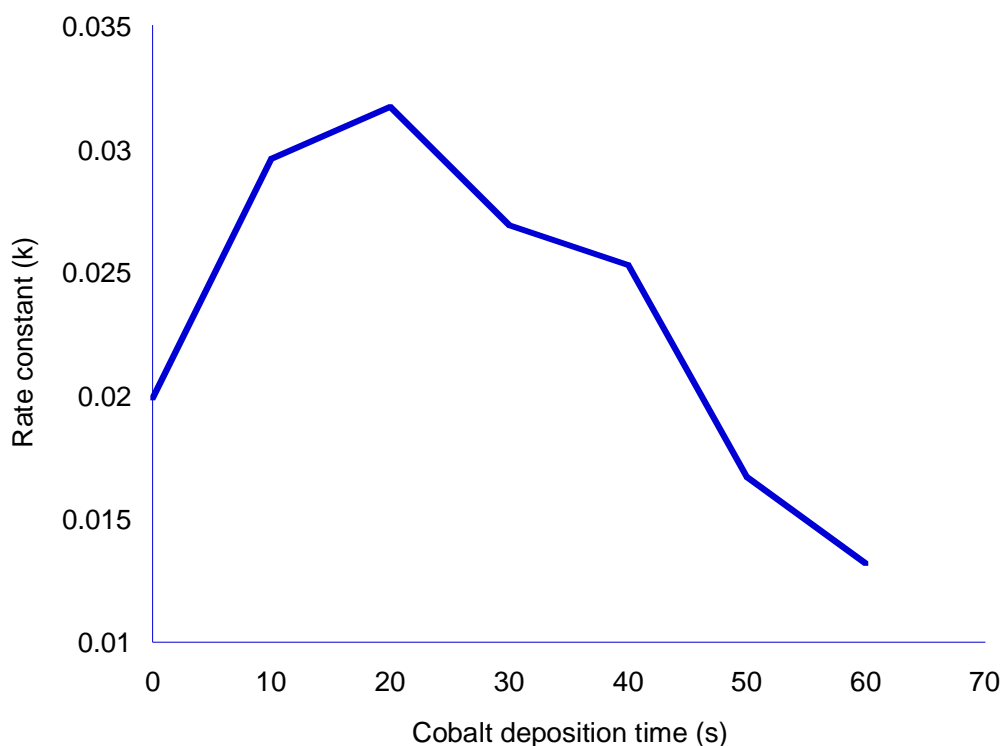


**Figure 22: Effect of pigment concentration on rate constant (k)**

The rate constant determines how fast the degradation takes place. The absorption edge shift in the reflectance spectra exhibited a reduction in the band gap in all the samples including those with higher Cobalt concentrations. The absorption coefficient and extinction coefficient



also showed more light absorption as the Cobalt concentration increases. It is therefore expected that the rate constant increases as the Cobalt concentration is increased. However, from figure 22 it is evident that the rate constants did not increase as expected but instead decreased after ZnO:Co 20s which could be due to the change in the *ZnO* grain size Cobalt concentration is further increased as observed by Sharma et al. (2016).

The highest rate constant was that at ZnO:Co 20s which was  $0.0317\text{hr}^{-1}$  This film had the optimum Cobalt concentration which enhances photocatalysis. The rate constants for ZnO:Co 10s, ZnO:Co 30s and ZnO:Co 40s were higher than that for pure *ZnO* an indication that Cobalt pigmentation enhanced the photocatalytic degradation of methylene blue. However, the rate constants for ZnO:Co 50s and ZnO:Co 60s were low compared to that of unpigmented *ZnO* showing a decrease in the photodegradation rate. This implied that higher Cobalt concentration reduced the degradation rate as stated earlier by Sutanto et al. (2017). It was therefore concluded that the best Cobalt concentration for anodized *ZnO* photocatalysis is obtained by depositing Cobalt in *ZnO* for 20s.

## **CHAPTER FIVE**

### **SUMMARY, CONCLUSIONS AND RECOMMENDATIONS**

#### **5.1 Introduction**

In the former chapters a report of the optical properties and photocatalytic performance of pure and Cobalt pigmented ZnO has been presented. In this chapter a summary of the study, conclusions made from the study and the recommendations are discussed.

#### **5.2 Summary**

Pure and Cobalt pigmented *ZnO* thin films were synthesized successfully by anodization. This method was used because of its simplicity, ease and cost effectiveness in the fabrication of films. A UV-VIS-NIR spectrophotometer was used to characterize optically the fabricated films and reflectance measurements were obtained. Data analysis was done using the SCOUT software which abetted in the determination of the optical constants of the films. The films performance on the degradation of methylene blue under UV radiation was investigated in its decolourisation which resulted in a decrease in its absorbance hence concentration. The films with a higher degradation rate were *ZnO* pigmented with Cobalt for 20s hence preferred to be used in photocatalytic water treatment.

#### **5.3 Conclusions**

##### **5.3.1 Fabrication of *ZnO***

*ZnO* thin films were successfully anodized in 0.5M oxalic acid at 10V for 60 minutes. A white *ZnO* film formed on the Zinc metal substrate. The *ZnO* film formed on the substrate in this method was uniformly spread on the substrate. The challenge however was on the

determination of the film thickness since the substrate used was opaque and its absorbance and thickness could not be measured directly but obtained by modelling.

### **5.3.2 Pigmenting *ZnO* with Cobalt**

*ZnO* films were pigmented with Cobalt at a constant voltage of 20V by electrodeposition method and the deposition time varied from 10s to 60s. When the time at which Cobalt was deposited was increased, the Cobalt concentration increased. The increase in Cobalt concentration is confirmed by Faraday's law of electrochemistry. The films became dark when Cobalt was incorporated and darkening intensified with increase in Cobalt concentration. In this study, *ZnO* films were said to be pigmented and not doped since doping involve formation of bonds between the semiconductor atoms and the impurity atoms but in this study no experiment was done to find out whether there was formation of bonds between *ZnO* and Cobalt even after post deposition heat treatment.

### **5.3.3 Determination of optical properties of pure and Cobalt pigmented *ZnO***

The properties obtained in optical characterization are reflectance, absorption coefficient, the refractive index, the extinction coefficient and the band gap energy of the fabricated films. Anodized *ZnO* films were observed to generally have a high reflectance but the reflectance decreased on pigmentation with Cobalt which led to an increase in absorption. Pigmentation led to a red shift of the absorption edge also confirming an escalation in absorption.

The absorption coefficient increased sharply at low wavelengths which corresponded to the films band gap energy of the films. This was however lower at longer wavelengths. Cobalt

concentration increases the absorption coefficient which further confirms increase in absorption.

Anodized ZnO refractive index and extinction coefficient was found to be low compared to those obtained using other methods which could be accredited to the *ZnO* film forming on the zinc substrate having a low density. The films may not be well packed and could be having voids hence the effects of the Zinc substrate exposed at the voids. This could also be as a result of the effects of the substrate since the films formed were thin. High Cobalt content in *ZnO* increased the extinction coefficient.

The *ZnO* optical band gap revealed a general decreasing trend from 3.34eV to 3.10eV as the Cobalt concentration was increased. The decrease in band gap confirmed the red shift observed in the absorption edge.

#### **5.3.4 Photocatalytic performance of unpigmented and Cobalt pigmented *ZnO***

The photocatalytic performance of pure and Cobalt pigmented *ZnO* films in methylene blue degradation under UV radiation showed an increase in photocatalytic activity with pigmentation. High Cobalt concentration however lowered the photocatalytic activity showing that there is an optimum Cobalt concentration required to enhance photocatalytic activity. *ZnO* with Cobalt deposited for 20s was the most photocatalytic hence has the optimum Cobalt concentration suitable for Cobalt pigmented *ZnO* photocatalytic water treatment.

#### 5.4 Recommendations for further research

- i) In the deposition of Cobalt in the *ZnO* films, darkening of the films was observed which was attributed to its incorporation into the *ZnO* crystal structure. Also, *ZnO* properties were observed to be altered upon introduction of Cobalt. The shift towards longer wavelengths in the absorption edge was assumed to be a result of substitution of  $Zn^{2+}$  ions by  $Co^{2+}$  ions which may not be the case since Cobalt may have just diffused into *ZnO* hence no bonding. It is therefore recommended that further studies should be done to find out if there was formation of bonds between Cobalt and *ZnO*.
  
- ii) The results obtained and reported in this work show a clear influence of the Cobalt concentration on *ZnO* optical properties and photocatalytic activity. This study was confined to a narrow study of the optical properties. Photocatalysis is also influenced by other factors like the structure and surface morphology. It is therefore recommended that structural characterization of the films be done to confirm the surface morphology and the crystal structure and orientation. This is studied using Scanning Electron Microscopy (SEM), Transmission Electron Microscopy (TEM) and X-ray Diffraction (XRD).
  
- iii) The reason for low refractive index and extinction coefficient was attributed to loosely packed films with voids. It is recommended that further studies on the nature of the film be done so as to determine whether that is actually the reason for the low optical constants.

iv) ZnO:Co 20s films were found to be the most photocatalytic regardless of the fact that Cobalt pigmentation increased the absorption of the films. This was attributed to partly the *ZnO* grain size as more Cobalt was deposited but this was not investigated. It is therefore recommended that further studies should be done on the effect of pigment concentration on the size of *ZnO* particles.

## REFERENCES

- Agus, S. G., Irmansyah, I., & Akhiruddin, M. (2016). Dye-sensitized Solar Cell Based on Flower-like ZnO Nanoparticles as Photoanode and Natural Dye as Photosensitizer. *Журнал нано-та електронної фізики*, (8, № 2), 02012-1.
- Anandan, S., & Miyauchi, M. (2011). Ce-doped ZnO ( $\text{Ce}_x\text{Zn}_{1-x}\text{O}$ ) becomes an efficient visible-light-sensitive photocatalyst by co-catalyst ( $\text{Cu}^{2+}$ ) grafting. *Physical Chemistry Chemical Physics*, 13(33), 14937-14945.
- Angulo Abanto, J. R. (2016). On the fundamental absorption of amorphous semiconductors.
- Asim, N., Ahmadi, S., Alghoul, M. A., Hammadi, F. Y., Saeedfar, K., & Sopian, K. (2014). Research and development aspects on chemical preparation techniques of photoanodes for dye sensitized solar cells. *International Journal of Photoenergy*, 2014.
- ASTM G173-03(2012), Standard Tables for Reference Solar Spectral Irradiances: Direct Normal and Hemispherical on  $37^\circ$  Tilted Surface, ASTM International, West Conshohocken, PA, 2012, referenced from <https://www.astm.org/Standards/G173.htm> on April 2019.
- Baghdad, R., Lemée, N., Lamura, G., Zeinert, A., Hadj-Zoubir, N., Bousmaha, M., ... & Zellama, K. (2017). Structural and magnetic properties of Co-doped ZnO thin films grown by ultrasonic spray pyrolysis method. *Superlattices and Microstructures*, 104, 553-569.
- Bahşi, Z. B., & Oral, A. Y. (2007). Effects of Mn and Cu doping on the microstructures and optical properties of sol-gel derived ZnO thin films. *Optical Materials*, 29(6), 672-678.
- Bakr, N. A., Salman, S. A., & Shano, A. M. (2015). Effect of co doping on structural and optical properties of NiO thin films prepared by chemical spray pyrolysis method. *International Letters of Chemistry, Physics and Astronomy*, 41, 15-30.
- Baruah, S., & Dutta, J. (2009). Hydrothermal growth of ZnO nanostructures. *Science and Technology of Advanced Materials*, 10(1), 013001.
- Basu, P. K., Saha, N., Maji, S., Saha, H., & Basu, S. (2008). Nanoporous ZnO thin films deposited by electrochemical anodization: effect of UV light. *Journal of Materials Science: Materials in Electronics*, 19(6), 493-499.
- Benno, Grolik, and Kopp Joachim. (2003) "Optical properties of thin semiconductor films." *October, 31st* (2003).
- Bhattacharyya, B. (2015). "Electrochemical micromachining for nanofabrication." *MEMS and Nanotechnology*, William Andrew Applied Science Publishers, Imprint of Elsevier Inc., Massachusetts: 270.
- Bloss, W. H., Pfisterer, F., & Schock, H. W. (1988). Advances in solar energy, an annual review of research and development. *Amer. Solar Energy Soc. Ic., New York*, 4, 275.
- Borhani Zarandi, M., & Amrollahi Bioki, H. (2017). Effects of Cobalt Doping on Optical Properties of ZnO Thin Films Deposited by Sol-Gel Spin Coating Technique. *Journal of Optoelectronic Nanostructures*, 2(4), 33-44.
- Cao, X., Wang, N., Wang, L., & Guo, L. (2010). Porous ZnO nanobelts: synthesis, mechanism, and morphological evolutions. *Journal of Nanoparticle Research*, 12(1), 143-150.
- Chandrappa, K. G., & Venkatesha, T. V. (2012). Electrochemical synthesis and photocatalytic property of zinc oxide nanoparticles. *Nano-Micro Letters*, 4(1), 14-24.

- Chen, L. C., Tu, Y. J., Wang, Y. S., Kan, R. S., & Huang, C. M. (2008). Characterization and photoreactivity of N-, S-, and C-doped ZnO under UV and visible light illumination. *Journal of Photochemistry and Photobiology A: Chemistry*, 199(2-3), 170-178.
- Chuah, L. S., Hassan, Z., & Bakhori, S. M. (2012, April). Nanoporous ZnO prepared by electrochemical anodization deposition. In *Third International Conference on Smart Materials and Nanotechnology in Engineering* (Vol. 8409, p. 84092E). International Society for Optics and Photonics.
- Depla, D., & Mahieu, S. (2008). *Reactive sputter deposition* (Vol. 109, p. 140). Berlin: Springer.
- Djordjevic, L., Primorac, M., Stupar, M., & Krajisnik, D. (2004). Characterization of caprylocaproyl macrogolglycerides based microemulsion drug delivery vehicles for an amphiphilic drug. *International Journal of Pharmaceutics*, 271(1-2), 11-19.
- Duffie, J. A., & Beckman, W. A. (1991). *Solar engineering of thermal processes* (pp. 770-772). New York: Wiley.
- El Ghouli, J., Kraini, M., & El Mir, L. (2015). Synthesis of Co-doped ZnO nanoparticles by sol-gel method and its characterization. *Journal of Materials Science: Materials in Electronics*, 26(4), 2555-2562.
- Ertl, G. (1990). Elementary steps in heterogeneous catalysis. *Angewandte Chemie International Edition in English*, 29(11), 1219-1227.
- Espitia, P. J. P., Soares, N. D. F. F., dos Reis Coimbra, J. S., de Andrade, N. J., Cruz, R. S., & Medeiros, E. A. A. (2012). Zinc oxide nanoparticles: synthesis, antimicrobial activity and food packaging applications. *Food and Bioprocess Technology*, 5(5), 1447-1464.
- Fabbiyola, S., Kennedy, L. J., Aruldoss, U., Bououdina, M., Dakhel, A. A., & JudithVijaya, J. (2015). Synthesis of Co-doped ZnO nanoparticles via co-precipitation: Structural, optical and magnetic properties. *Powder Technology*, 286, 757-765.
- Friz, M., & Waibel, F. (2003). Coating materials. In *Optical interference coatings* (pp. 105-130). Springer, Berlin, Heidelberg.
- Fujishima, A., Hashimoto, K., & Watanabe, T. (1999). *TiO<sub>2</sub> Photocatalysis*, Bkc. Inc.: Tokyo, Japan.
- Fujishima, A., Rao, T. N., & Tryk, D. A. (2000). Titanium dioxide photocatalysis. *Journal of photochemistry and photobiology C: Photochemistry reviews*, 1(1), 1-21.
- Gajbhiye, S. B. (2012). Photocatalytic degradation study of methylene blue solutions and its application to dye industry effluent. *Int. J. Mod. Eng. Res*, 2(3), 1204-1208.
- Gallarate, M., Carlotti, M. E., Trotta, M., & Ugazio, E. (2004). Disperse systems as topical formulations containing alfa-tocopherol. *Journal of Drug Delivery Science and Technology*, 14, 471-477.
- Ghorani-Azam, A., Riahi-Zanjani, B., & Balali-Mood, M. (2016). Effects of air pollution on human health and practical measures for prevention in Iran. *Journal of research in medical sciences: the official journal of Isfahan University of Medical Sciences*, 21.
- Gilani, S., Ghorbanpour, M., & Jadid, A. P. (2016). Antibacterial activity of ZnO films prepared by anodizing. *Journal of Nanostructure in Chemistry*, 6(2), 183-189.
- Goswami, D. Y. (1995). *Advances in Solar Energy: An Annual Review of Research and Development*, edited by K. W. Böer, American Solar Energy Society, Boulder, U.S.A., 1995, Vol. 10, pp. 165-209.
- Goswami, D. Y. (2007). *Advances in Solar Energy: an Annual Review of Research and Development* (Vol. 17). Earthscan.



- Gupta V, Mansingh A. (1996). Influence of post deposition annealing on the structural and optical properties of sputtered zinc oxide film. *J Appl phys* 1996;80 (2):1063–73.
- Herrmann, J. M. (2005). Heterogeneous photocatalysis: state of the art and present applications In honor of Pr. RL Burwell Jr.(1912–2003), Former Head of Ipatieff Laboratories, Northwestern University, Evanston (Ill). *Topics in catalysis*, 34(1-4), 49-65.
- Hoffmann, M. R., Martin, S. T., Choi, W., & Bahnemann, D. W. (1995). Environmental applications of semiconductor photocatalysis. *Chemical reviews*, 95(1), 69-96.
- Holden T., Ram P., Pollak H., Freeouf J., Yang B., Tamargo M., (1997). *Phys.Rev.* B56, 4037.
- Huang M.H, S. Mao, H. Feick, H. Yan, Y. Wu, H. Kind, E. Weber, R. Russo, and P. Yang, (2001) *Science* 292, 1897.
- Imam, M. A., Moniruzzaman, M., & Mamun, M. A. (2011, November). Anodizing of zinc for improved surface properties. In *Proceedings of a meeting held* (pp. 20-24).
- Iqbal, J., Janjua, R. A., & Jan, T. (2014). Structural, optical and magnetic properties of Co-doped ZnO nanoparticles prepared via a wet chemical route. *International Journal of Modern Physics B*, 28(25), 1450158.
- Iqbal, J., Jilani, A., Hassan, P. Z., Rafique, S., Jafer, R., & Alghamdi, A. A. (2016). ALD grown nanostructured ZnO thin films: Effect of substrate temperature on thickness and energy band gap. *Journal of King Saud University-Science*, 28(4), 347-354.
- Irani, M., Mohammadi, T., & Mohebbi, S. (2016). Photocatalytic degradation of methylene blue with ZnO nanoparticles; a joint experimental and theoretical study. *Journal of the Mexican Chemical Society*, 60(4), 218-225.
- Jain, A., Sagar, P., & Mehra, R. M. (2006), Band gap widening and narrowing in moderately and heavily doped n-ZnO films. *Solid. State. Electron.* 50(7-8), 1420-1424.
- Janotti, A., & Van de Walle, C. G. (2009). Fundamentals of zinc oxide as a semiconductor. *Reports on progress in physics*, 72(12), 126501.
- Joshi, B., Saxena, P., & Khera, N. (2016, March). Optical properties of Zinc oxide (ZnO) thin films for applications in optical devices: MATLAB Simulation. In *2016 3rd International Conference on Computing for Sustainable Global Development (INDIACom)* (pp. 2261-2265). IEEE.
- Kalpana, S., Krishnan, S. S., Senthil, T. S., & Elangovan, S. V. (2017). COBALT DOPED ZINC OXIDE NANOPARTICLES FOR PHOTOCATALYTIC APPLICATIONS. *Journal of Ovonic Research Vol*, 13(5), 263-269.
- Kao, C. Y., Liao, J. D., Chang, C. W., & Wang, R. Y. (2011). Thermal diffusion of Co into sputtered ZnO: Co thin film for enhancing visible-light-induced photo-catalytic activity. *Applied Surface Science*, 258(5), 1813-1818.
- Kaushik, A., Dalela, B., Rathore, R., Vats, V. S., Choudhary, B. L., Alvi, P. A., ... & Dalela, S. (2013). Influence of Co doping on the structural, optical and magnetic properties of ZnO nanocrystals. *Journal of Alloys and Compounds*, 578, 328-335.
- Khelladi, N. B., & Sari, N. C. (2013). Optical properties of ZnO thin film. *Advances in Materials Sciences*, 13(1), 21-29.
- Klosek, S., & Raftery, D. (2001). Visible light driven V-doped TiO<sub>2</sub> photocatalyst and its photooxidation of ethanol. *The Journal of Physical Chemistry B*, 105(14), 2815-2819.

- Kong, X. Y., & Wang, Z. L. (2003). Spontaneous polarization-induced nanohelices, nanosprings, and nanorings of piezoelectric nanobelts. *Nano Letters*, 3(12), 1625-1631.
- Kudo, A., & Miseki, Y. (2009). Heterogeneous photocatalyst materials for water splitting. *Chemical Society Reviews*, 38(1), 253-278.
- Kulkarni, S. S., & Shirsa, M. D. (2015). Optical and structural properties of zinc oxide nanoparticles. *IJARPS*, 2, 14-18.
- Kuriakose, S., Satpati, B., & Mohapatra, S. (2014). Enhanced photocatalytic activity of Co doped ZnO nanodisks and nanorods prepared by a facile wet chemical method. *Physical Chemistry Chemical Physics*, 16(25), 12741-12749.
- Lavand, A. B., & Malghe, Y. S. (2015). Synthesis, characterization and visible light photocatalytic activity of nitrogen-doped zinc oxide nanospheres. *Journal of Asian Ceramic Societies*, 3(3), 305-310.
- Lee, J., Hui, K. N., Hui, K. S., Cho, Y. R., & Chun, H. H. (2014). Low resistivity of Ni–Al co-doped ZnO thin films deposited by DC magnetron sputtering at low sputtering power. *Applied Surface Science*, 293, 55-61.
- Li, W., Wang, G., Chen, C., Liao, J., & Li, Z. (2017). Enhanced visible light photocatalytic activity of ZnO nanowires doped with Mn<sup>2+</sup> and Co<sup>2+</sup> ions. *Nanomaterials*, 7(1), 20.
- Lizama, C., Freer, J., Baeza, J., & Mansilla, H. D. (2002). Optimized photodegradation of Reactive Blue 19 on TiO<sub>2</sub> and ZnO suspensions. *Catalysis Today*, 76(2-4), 235-246.
- Luo, Q., Xu, P., Qiu, Y., Cheng, Z., Chang, X., & Fan, H. (2017). Synthesis of ZnO tetrapods for high-performance supercapacitor applications. *Materials Letters*, 198, 192-195.
- Macleod, H. A. (1969). *Thin Film Optical Filters* McGraw-Hill, Hilger, London, Vol. II, 38-40.
- Madhusoodanan, K. N., Vimalkumar, T. V., & Vijayakumar, K. P. (2015). Gas sensing application of nanocrystalline zinc oxide thin films prepared by spray pyrolysis. *Bulletin of Materials Science*, 38(3), 583-591.
- Maeda, K. (2011). Photocatalytic water splitting using semiconductor particles: history and recent developments. *Journal of Photochemistry and Photobiology C: Photochemistry Reviews*, 12(4), 237-268.
- Maghanga, C. M., & Mwamburi, M. M. (2018). Contribution of Drude and Brendel Model Terms to the Dielectric Function; A case of TiO<sub>2</sub>: Nb Thin Films. *Journal of Modeling and Simulation of Materials*, 1(1), 3-7.
- Makuku, O., Mbaiwa, F., & Sathiaraj, T. S. (2016). Structural, optical and electrical properties of low temperature grown undoped and (Al, Ga) co-doped ZnO thin films by spray pyrolysis. *Ceramics International*, 42(13), 14581-14586.
- Masuda, H., & Fukuda, K. (1995). Ordered metal nanohole arrays made by a two-step replication of honeycomb structures of anodic alumina. *science*, 268(5216), 1466-1468.
- Mathew, J. P., Varghese, G., & Mathew, J. (2015). Effect of Annealing on the Optical Properties of Transition Metal Doped ZnO Thin Films. In *IOP Conference Series: Materials Science and Engineering* (Vol. 73, No. 1, p. 012065). IOP Publishing.
- Meenakshi, G., & Sivasamy, A. (2017). Synthesis and characterization of zinc oxide nanorods and its photocatalytic activities towards degradation of 2, 4-D. *Ecotoxicology and environmental safety*, 135, 243-251.

- Mwamburi, M., & Wäckelgård, E. (2000). Doped tin oxide coated aluminium solar selective reflector surfaces. *Solar Energy*, 68(4), 371-378.
- Nagaraju, G., Shivaraju, G. C., Banuprakash, G., & Rangappa, D. (2017). Photocatalytic activity of ZnO nanoparticles: synthesis via solution combustion method. *Materials Today: Proceedings*, 4(11), 11700-11705.
- Nemes, D., Moldovan, V., Bruj, E., Jumate, N., & Vida-Simiti, I. (2011). Porous anodic alumina films obtained by two step anodization. *Bulletin of the Transilvania University of Brasov. Engineering Sciences. Series I*, 4(2), 75.
- Ng, S. W., Yam, F. K., Low, L. L., Beh, K. P., Mustapha, M. F., Sota, E. N., ... & Hassan, Z. (2011). Self-assembled ZnO nanostripes prepared by acidified ethanolic anodization. *Optoelectron Adv Mat-rapid communications*, 5, 89-91.
- Ong, C. B., Ng, L. Y., & Mohammad, A. W. (2018). A review of ZnO nanoparticles as solar photocatalysts: Synthesis, mechanisms and applications. *Renewable and Sustainable Energy Reviews*, 81, 536-551.
- Oves, M., Arshad, M., Khan, M. S., Ahmed, A. S., Azam, A., & Ismail, I. M. (2015). Anti-microbial activity of cobalt doped zinc oxide nanoparticles: targeting water borne bacteria. *Journal of Saudi Chemical Society*, 19(5), 581-588.
- Palik, E. D. (Ed.). (1998). *Handbook of optical constants of solids* (Vol. 3). Academic press.
- Pankove, J. I. (1971). Optical processes on semiconductors Dover publication. *Inc. New york*.
- Patil, P. S. (1999). Versatility of chemical spray pyrolysis technique. *Materials Chemistry and physics*, 59(3), 185-198.
- Polyanskiy, M. N. "Refractive index database," <https://refractiveindex.info>. Accessed on 2019-03-22.
- Poongodi, G., Anandan, P., Kumar, R. M., & Jayavel, R. (2015). Studies on visible light photocatalytic and antibacterial activities of nanostructured cobalt doped ZnO thin films prepared by sol-gel spin coating method. *Spectrochimica Acta Part A: Molecular and Biomolecular Spectroscopy*, 148, 237-243.
- Prihod'ko, R. V., & Soboleva, N. M. (2013). Photocatalysis: oxidative processes in water treatment. *Journal of Chemistry*, 2013.
- Pung, S. Y. (2010). Synthesis and characterization of zinc oxide nanowires (Doctoral dissertation, University of Nottingham).
- Qin, H. P., Su, Q., Khu, S. T., & Tang, N. (2014). Water quality changes during rapid urbanization in the Shenzhen River Catchment: An integrated view of socio-economic and infrastructure development. *Sustainability*, 6(10), 7433-7451.
- Rathod, J. R. (2014). Investigations on the growth and characterization of znTe thin films deposited by Silar method for possible window applications.
- Rochman, N. T., & Akwalia, P. R. (2017, May). Fabrication and characterization of Zinc Oxide (ZnO) nanoparticle by sol-gel method. In *Journal of Physics: Conference Series* (Vol. 853, No. 1, p. 012041). IOP Publishing.
- Rodríguez-de Marcos, L. V., & Larruquert, J. I. (2016). Analytic optical-constant model derived from Tauc-Lorentz and Urbach tail. *Optics express*, 24(25), 28561-28572.
- Salager, J. L., Marquez, N., Graciaa, A., & Lachaise, J. (2000). Partitioning of ethoxylated octylphenol surfactants in microemulsion- oil- water systems: Influence of temperature and relation between partitioning coefficient and physicochemical formulation. *Langmuir*, 16(13), 5534-5539.

- Samanta, P. K., Patra, S. K., Ghosh, A., & Chaudhuri, P. R. (2009). Visible emission from ZnO nanorods synthesized by a simple wet chemical method. *Int. J. Nanosci. Nanotechnol*, 1(1-2), 81-90.
- Sharma, D., Rajput, J., Kaith, B. S., Kaur, M., & Sharma, S. (2010). Synthesis of ZnO nanoparticles and study of their antibacterial and antifungal properties. *Thin solid films*, 519(3), 1224-1229.
- Sharma, N., Thakur, S., Sharma, R., & Kumar, J. (2016). Effect of Cobalt Doping on Physical Properties of ZnO Nanoparticles. *CPUH-Res. J*, 1, 47-51.
- Shetty, A., & Nanda, K. K. (2012). Synthesis of zinc oxide porous structures by anodization with water as an electrolyte. *Applied Physics A*, 109(1), 151-157.
- Suryawanshi, H. P., Bachhav, S. G., & Patil, D. R. (2015). Hydrothermal synthesis of zinc oxide and its photocatalytic effect. *IJCPS*, 4, 483-486.
- Sutanto, H., Wibowo, S., Arifin, M., & Hidayanto, E. (2017). Photocatalytic activity of cobalt-doped zinc oxide thin film prepared using the spray coating technique. *Materials Research Express*, 4(7), 076409.
- Tan, T. R., Cheng, J. R., Wang, J. H., Duh, J. G., & Shih, H. C. (1998). Morphology and characterization of the anodic coating on galvanized steels prepared by alternating currents. *Surface and Coatings Technology*, 110(3), 194-199.
- Taylor JL. Design Considerations of Small (60 mm) Vs. Large (150 mm) Integrating Spheres. Application Note. Shelton: Perkin Elmer; 2010.
- Theiss, W. (2000) in *Scout Thin Film Analysis Software Handbook*, edited by M. Theiss (Hard-and Software, Aachen, Germany).
- UNICEF (2008). *The state of the world's children: maternal and newborn health* (Vol. 9). Unicef.
- UNICEF WHO (2014) Joint Water Supply, & Sanitation Monitoring Programme. *Progress on drinking water and sanitation: World Health Organization*.
- UNWWAP (United Nations World Water Assessment Programme) (2016). *The United Nations World Water Development Report, Paris, France:* (pp. 1–148).
- Vanaja, A., & Rao, K. S. (2016). Effect of Co Doping on Structural and Optical Properties of Zinc Oxide Nanoparticles Synthesized by Sol-Gel Method. *Advances in Nanoparticles*,
- Vinu, R., & Madras, G. (2012). Environmental remediation by photocatalysis. *Journal of the Indian Institute of Science*, 90(2), 189-230.
- Voon, C. H., Derman, M. N., Hashim, U., & Foo, K. L. (2014). Effect of Anodizing Voltage on the Formation of Porous Anodic Alumina on Al-0.5 wt% Mn Alloys. In *Advanced Materials Research* (Vol. 925, pp. 455-459). Trans Tech Publications.
- Voon, C. H., Derman, M. N., Hashim, U., Lim, B. Y., Sam, S. T., Foo, K. L., & Ten, S. T. (2015). Synthesis of nanoporous zinc oxide by anodizing of zinc in distilled water. *Applied Mechanics and Materials*, 754, 1126.
- Wahab, H. A., Salama, A. A., El-Saeid, A. A., Nur, O., Willander, M., & Battisha, I. K. (2013). Optical, structural and morphological studies of (ZnO) nano-rod thin films for biosensor applications using sol gel technique. *Results in Physics*, 3, 46-51.
- Woo, H. S., Kwak, C. H., Chung, J. H., & Lee, J. H. (2014). Co-doped branched ZnO nanowires for ultraselective and sensitive detection of xylene. *ACS applied materials & interfaces*, 6(24), 22553-22560.

- Xie, Y., He, Y., Irwin, P. L., Jin, T., & Shi, X. (2011). Antibacterial activity and mechanism of action of zinc oxide nanoparticles against *Campylobacter jejuni*. *Applied and environmental microbiology*, 77(7), 2325-2331.
- Xu, Y., Jin, J., Li, X., Han, Y., Meng, H., Wang, T., & Zhang, X. (2016). Simple synthesis of ZnO nanoflowers and its photocatalytic performances toward the photodegradation of metamitron. *Materials Research Bulletin*, 76, 235-239.
- Yamaguchi, Y., Yamazaki, M., Yoshihara, S., & Shirakashi, T. (1998). Photocatalytic ZnO films prepared by anodizing. *Journal of Electroanalytical Chemistry*, 442(1-2), 1-3.
- Yildirim, O. A., Arslan, H., & Sönmezoğlu, S. (2016). Facile synthesis of cobalt-doped zinc oxide thin films for highly efficient visible light photocatalysts. *Applied Surface Science*, 390, 111-121.
- Young, M. I. (2016). *Synthesis of zinc oxide nanoparticles with different morphologies by wet chemistry routes* (Doctoral dissertation, © Michael Young).
- Yousif, A. A., Habubi, N. F., & Haidar, A. A. (2012). Nanostructure zinc oxide with cobalt dopant by PLD for gas sensor applications.
- Zhang, G., Shen, X., & Yang, Y. (2011). Facile synthesis of monodisperse porous ZnO spheres by a soluble starch-assisted method and their photocatalytic activity. *The Journal of Physical Chemistry C*, 115(15), 7145-7152.
- Zhang, X. L., Hui, K. N., Hui, K. S., & Singh, J. (2013). Structural and optical characterization of high-quality ZnO thin films deposited by reactive RF magnetron sputtering. *Materials Research Bulletin*, 48(3), 1093-1098.
- Zia, A., Shah, N. A., Ahmed, S., & Khan, E. U. (2014). The influence of cobalt on the physical properties of ZnO nanostructures. *Physica Scripta*, 89(10), 105802.

## APPENDICES

### Appendix 1: Cobalt Deposit and Methylene Blue Standard Solution Data

Data showing the amount of Cobalt deposited in ZnO films at varying deposition time and the integrated reflectance of the films

<b>Cobalt Deposition Time (Seconds)</b>	<b>Amount of Cobalt Deposited (Grams)</b>	<b>Integrated (Average) Reflectance (%)</b>
0.0000	0.0000	48.78
10.000	0.0067	47.77
20.000	0.0130	43.76
30.000	0.0200	42.88
40.000	0.0270	38.53
50.000	0.0330	37.80
60.000	0.0400	32.87

### Calibration Data on Methylene Blue Standard Solution

<b>Concentration (ppm)</b>	<b>Absorbance</b>
0.0000	0.0000
2.0000	0.5370
4.0000	1.0610
6.0000	1.5300
8.0000	1.9700
10.000	2.4130

## Appendix 2: Kabarak University Introductory Letter



### INSTITUTE OF POST GRADUATE STUDIES

Private Bag - 20157  
KABARAK, KENYA  
E-mail: [directorpostgraduate@kabarak.ac.ke](mailto:directorpostgraduate@kabarak.ac.ke)

Tel: 0203511275  
Fax: 254-51-343012  
[www.kabarak.ac.ke](http://www.kabarak.ac.ke)

13<sup>rd</sup> Aug, 2018

TO WHOM IT MAY CONCERN

Dear Sir/Madam,

**RE: RESEARCH BY JUDITH CHEBWOGEN – GMP/M/2394/11/16**

The above named is a student at Kabarak University taking Masters Degree in Physics. She has successfully defended her proposal entitled “*Fabrication and Characterization of Anodized Doped Zinc for Photocatalytic Application.*” She is therefore allowed to proceed for data collection and report writing.

Any assistance accorded to her is highly appreciated.

Thank you.

Yours faithfully,

**Dr. Betty J. Tikoko**  
**DIRECTOR - (POST-GRADUATE STUDIES)**



---

#### Kabarak University Moral Code

*As members of Kabarak University family, we purpose at all times and in all places, to set apart in one's heart, Jesus as Lord. (1 Peter 3:15)*




Kabarak University is ISO 9001:2015 Certified

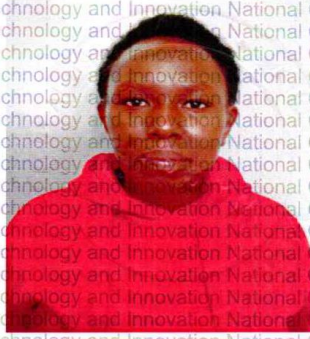
### Appendix 3: Nacosti Introductory Letter

THIS IS TO CERTIFY THAT:  
**MS. JUDITH CHEBWOGEN**  
of **KABARAK UNIVERSITY, 0-20200**  
**KERICHO, has been permitted to conduct**  
**research in All Counties**  
on the topic: **FABRICATION AND**  
**CHARACTERIZATION OF ANODIZED**  
**DOPED ZINC FOR PHOTOCATALYTIC**  
**APPLICATION**  
for the period ending:  
**25th July, 2020**

**Permit No : NACOSTI/P/19/84181/31263**  
**Date Of Issue : 26th July, 2019**  
**Fee Recieved : Ksh 1000**

  
**Director General**  
**National Commission for Science,**  
**Technology & Innovation**

**Applicant's**  
**Signature**





## Appendix 4: Nacosti Permit Research



### NATIONAL COMMISSION FOR SCIENCE, TECHNOLOGY AND INNOVATION

Telephone: +254-20-2213471,  
2241349, 3310571, 2219420  
Fax: +254-20-318245, 318249  
Email: dg@nacosti.go.ke  
Website: www.nacosti.go.ke  
When replying please quote

NACOSTI, Upper Kabete  
Off Waiyaki Way  
P.O. Box 30623-00100  
NAIROBI-KENYA

Ref. No. **NACOSTI/P/19/84181/31263**

Date: **26<sup>th</sup> July, 2019**

Judith Chebwogen  
Kabarak University  
Private Bag - 20157  
**KABARAK.**

#### **RE: RESEARCH AUTHORIZATION**

Following your application for authority to carry out research on "*Fabrication and characterization of anodized doped zinc for photocatalytic application.*" I am pleased to inform you that you have been authorized to undertake research in **all Counties** for the period ending **25<sup>th</sup> July, 2020.**

You are advised to report to **the County Commissioners, the County Directors of Health Services, and the County Directors of Education, all Counties** before embarking on the research project.

Kindly note that, as an applicant who has been licensed under the Science, Technology and Innovation Act, 2013 to conduct research in Kenya, you shall deposit **a copy** of the final research report to the Commission within **one year** of completion. The soft copy of the same should be submitted through the Online Research Information System.

**GODFREY P. KALERWA., MSc, MBA, MKIM  
FOR: DIRECTOR-GENERAL/CEO**

Copy to:

The County Commissioners  
All Counties.

The County Directors of Education  
All Counties.

## Appendix 5: Research Affiliation Approval

  
**THE UNIVERSITY OF ZAMBIA**  
**DIRECTORATE OF RESEARCH AND GRADUATE STUDIES**  
**RESEARCH DEPARTMENT**

Telephone: +260-211-290258/293937  
Fax: +260-1-290258/293937  
E-mail: drgs@unza.zm

P O Box 32379  
Lusaka, Zambia  
Your Ref:

---

**Kenyan Nationality, passport number AK0057133 valid until 17.01.2028**

5<sup>th</sup> December, 2018

Ms. Judith Chebwogen,  
P. O. Box 1479-20200,  
Kericho,  
Kenya.

Dear Ms. Judith Chebwogen,

**APPLICATION FOR RESEARCH AFFILIATION**

I am pleased to inform you that the University of Zambia, through the Directorate of Research and Graduate Studies (UNZA DRGS) has approved your application for research affiliation. You have been affiliated to the School of Natural Sciences, in the Department of Chemistry from 15<sup>th</sup> November, 2018 to 15<sup>th</sup> April, 2019. This will enable you to conduct your research entitled **"Fabrication and Characterization of Anodized Doped Zinc for Photocatalytic Application"**.

As a Research Affiliate at the University of Zambia you are obliged to contribute to participating in research seminars and conferences, depositing copies of research notes (including tapes, photos, etc.) in the University Library. You are also required to submit period report on the work being carried out.

Note that you are expected to deposit in the University Library one copy of any publication arising from work carried out during the period of affiliation and to acknowledge the assistance of the University in every such publication.

You are also required to apply for ethical clearance with the University of Zambia Research Ethics Committee before you proceed with your research here in Zambia.

I wish you every success in your research.

Yours Sincerely,

  
Alice M. Mweetwa (Dr.)  
**ASSISTANT DIRECTOR (RESEARCH) – DRGS**

  
UNIVERSITY OF ZAMBIA  
ASSISTANT DIRECTOR  
RESEARCH  
05 DEC 2018  
GRADUATE STUDIES  
P.O. BOX 32379, LUSAKA

Cc     Director – Directorate of Research and Graduate Studies  
       Dean – School of Natural Sciences  
       Head – Department of Chemistry  
       Assistant Registrar - Directorate of Research and Graduate Studies (Research)  
       Senior Administrative Officer - Directorate of Research and Graduate Studies (Affiliation)